

# (P)reheating after minimal Plateau Inflation and constraints from CMB

Debaprasad Maity and Pankaj Saha

Department of Physics,  
Indian Institute of Technology Guwahati,  
Guwahati, Assam, India 781039

E-mail: [debu@iitg.ac.in](mailto:debu@iitg.ac.in), [pankaj.saha@iitg.ac.in](mailto:pankaj.saha@iitg.ac.in)

**Abstract.** We have studied the preheating phase for a class of plateau inflationary model considering the four-legs interaction term  $(1/2)g^2\phi^2\chi^2$  between the inflaton ( $\phi$ ) and reheating field ( $\chi$ ). We specifically focus on the detailed effect of a parameter  $\phi_*$  that controls inflationary dynamics and the shape of the inflaton potential. For  $\phi_* < M_p$ , the departure of the inflaton potential from the usual power-law behavior  $\phi^n$  significantly modifies the microscopic behavior of the preheating dynamics. We analyze and compare in detail the efficiency of production, thermalization and the final equation of state of the system for different models under consideration with  $n = 2, 4, 6$  for two different values of  $\phi_*$ . Most importantly as we increase  $n$ , or decrease  $\phi_*$ , the preheating occurs very efficiently with the final equation of state to be that of the radiation,  $w = 1/3$ . Specially for  $n = 2$ , the final equation of state turned out to be  $w \simeq 0.2$ . However, a complete decay of inflaton could not be achieved with the four-legs interaction for any model under consideration. Therefore, in order to complete the reheating process, we perform the perturbative analysis for the second stage of the reheating phase. Taking the end product of the preheating phase as an initial condition we have solved the homogeneous Boltzmann equations for both the fields supplemented by the constraints coming from the subsequent entropy conservation. In so doing, we are able to calculate the reheating temperature which is otherwise ill-defined right after the end of preheating. The temperature can be uniquely fixed for a given inflaton decay constant and the CMB temperature. We also compare our results with the conventional reheating constraint analysis and discuss the limit of inflaton decay constant from the field theory perspective.

**Keywords:** Inflation, Preheating, Parametric resonance, Lattice simulation

---

## Contents

<b>1</b>	<b>Introduction</b>	<b>2</b>
<b>2</b>	<b>A Brief Introduction to the Minimal Inflation Model</b>	<b>4</b>
<b>3</b>	<b>Preheating: Parametric resonance</b>	<b>4</b>
3.0.1	Parametric resonance	4
<b>4</b>	<b>Stability-Instability chart: Analytic Treatment</b>	<b>6</b>
<b>5</b>	<b>Preheating: Lattice Simulation</b>	<b>7</b>
5.1	The Model and equations	7
<b>6</b>	<b>Analysis and Results</b>	<b>9</b>
6.1	The back-reaction and the emergence of non-linearity	9
6.1.1	General description of figures and results	10
6.1.2	$n = 2$	11
6.1.3	$n = 4$	13
6.1.4	$n = 6$	14
6.2	Equation of state	15
6.3	Occupation Numbers	18
6.4	Perturbative reheating and constraints from CMB	22
<b>7</b>	<b>Conclusion and Outlook</b>	<b>26</b>
<b>8</b>	<b>Acknowledgement</b>	<b>28</b>

---

## 1 Introduction

Inflation is a period in the early universe when the universe expanded exponentially in a quasi-vacuum like state void of any entropy or particles[1–6]. This exponential expansion during the inflation is the reason for the remarkable homogeneity of the cosmic microwave background(CMB). The inflationary mechanism is also responsible for generating the seed of all the large-scale structure in the universe. This period of inflation needs a state of negative pressure that can be easily achieved by a scalar field. Despite significant progress in the model independent analysis from effective field theories[7–10], inflation is still largely a model dependent phenomenon. In principle, any scalar field potential satisfying the well-known ‘*slow-roll*’ conditions can yield inflation. The list of models in inflationary cosmology is thus practically inexhaustible[12]. Nonetheless, the measurements of CMB anisotropies act as a probe for inflationary models. The PLANCK[13] and Keck Array, and BICEP2 Collaborations[14], result on inflationary parameters constraint the scalar spectral index as  $n_s = 0.968 \pm 0.006$ , and the scale dependence of scalar spectral index is tightly constrained parametrized by spectral running  $dn_s/d\ln k = -0.003 \pm 0.007$ . The upper bound on the tensor-to-scalar ratio, for 95 GHz Data From Keck Array, is  $r_{0.05} < 0.07$ (95 % CL). With these results a lot of simple and prominent models, for instance, the single field chaotic inflation models are currently ruled out. The models predicting smaller values of tensor-to-scalar ratio are now favored. One such model from super-gravity which also unifies a large class of inflationary models is known as the  $\alpha$ -attractor model. The potentials of these models are characterized by an infinite plateau for large field value with the minimum at the origin. The shape of the plateau can be controlled by a parameter called  $\alpha$  which can be chosen to reproduce the inflationary observables within the PLANCK limit. In our recent work[15] we have proposed a class of inflationary model which belong to a different class as compared to  $\alpha$ -attractor. The form of the potential resembles that of the power-law chaotic models with a non-minimal modification. The inflationary predictions and dynamics of those models have been discussed in details [15]. The reheating constraints on the model through CMB and dark matter abundance has also been studied[17] considering the perturbative reheating phenomena. The study of perturbative reheating with a phenomenological term with inflaton decay constant  $\Gamma_\phi$  is simple and convenient to understand several important aspects of the reheating phase especially the connection between CMB and the present dark matter abundance through the reheating temperature. However, this treatment relies on several assumptions on the nature of the reheating processes: (i) The first assumption is the absence of non-perturbative phenomena such as parametric resonance during reheating phase. Although the parametric resonance can be suppressed by choosing small enough value of the coupling parameter. However, it would be more appropriate to consider the perturbative reheating as a final stage of the whole reheating process with the initial conditions set by preheating stage. (ii) The second assumption is that we have also ignored the phenomena of inflaton fragmentation and the growth of inhomogeneity in the inflaton sector. With this the inflaton equation of state for the whole period of reheating has been described by that of the homogeneous inflaton condensate. For potentials  $V(\phi) \sim \phi^n$  near the minimum, using the virial theorem, the average equation of state are found to be  $w_\phi = (n - 2)/(n + 2)$ . It is needless to say that in any realistic reheating scenario the above assumptions have limited applicability. In this paper we have studied the non-linear effects of preheating and thermalization and then look into by perturbative reheating for the class of minimal plateau models we proposed recently.

The effects of parametric resonance is well studied in classical mechanics[26]. The importance of resonant particle production at the initial stage of reheating has been recognized and studied extensively for the first time in the seminal works of Kofman, Linde, and Starobinsky[22, 24]. The structure of resonance in the class of conformally invariant theories such as  $(\lambda/4)\phi^4 + (g^2/2)\phi^2\chi^2$  has been developed in [25]. It has been understood that the analytic study of preheating does not capture the full non-linear dynamics of this phase. A full non-linear study of non-perturbative field theory is needed for. However, if the occupation number of the different species is much larger than one we may study the system by ignoring their quantum nature[44, 45] and solving the appropriate classical wave equations. This fact serves as the basis for studying the preheating phase in  $3 + 1$  dimensional lattice. With the advent of different lattice codes[38, 46–48], lattice simulation study of preheating becomes quite frequent in the literature (see refs.([28, 29]) for a review and references therein). Another important aspect of preheating is the study of self resonance after inflation. In this case the inflaton quanta may become unstable due to small spatial perturbations even without coupling to other fields. The self-resonance is found to be inefficient for the case of chaotic models[25], however they can be efficient for multifield inflation[52, 53] or in the case of plateau type potentials[42, 54].

In this work we have studied the preheating and subsequent thermalization after minimal plateau inflation introduced in our earlier work[15]. The models predict small values of the scalar-to-tensor ratio( $r$ ) to be in agreement with the limit set by recent observations[13]. The class of models is parameterized by power  $n$  of the inflaton field  $\phi$  and most importantly a scale  $\phi_*$  that controls the energy scale of inflation, similar to the  $\alpha$  parameter for  $\alpha$ -attractor. The study of self-resonance phenomena with  $\alpha$ -attractor type potentials has been performed in [42, 54]. However, in any realistic model of preheating the inflaton coupled with other matter fields must be incorporated. The study of preheating when other matter fields are coupled has not been done in the literature for general plateau type of potentials. Therefore, in this paper we will consider the class of minimal plateau inflation models mentioned before. We will study in detail how particle production and the subsequent thermalization process depend on the scale  $\phi_*$  and the power of the potential  $n$ . The end of preheating can be identified around the scale factor where average value of all the energy component tend to become constant. Interestingly for  $n > 2$  all the models lead to effective equation of state equal to that of the radiation  $w = 1/3$ .

Another interesting observation is that the inflaton decay is not complete for any of the model considered here with a four-legs interaction. Therefore, as a logical next step we study the perturbative reheating process considering a phenomenological inflaton decay term into the Boltzmann equations for the inflaton and the reheating field. The phase of perturbative reheating enables us to connect the reheating phase with the current CMB date in terms of the primordial spectral index of the inflaton fluctuation. For a particular inflation model, the preheating dynamics turned out to be insensitive to the inflationary e-folding number which is a function of scalar spectral index. As a consequence in determining the reheating temperature the effect of preheating appears only through its e-folding number. Finally we have commented on the range of value of the coupling parameter that will set the value of the above perturbative inflaton decay term. Although, this work concerns with the above plateau potentials, the general conclusions in this work will be applicable to any other class of plateau potential having a controlling scale similar to  $\phi_*$  or  $\alpha$ .

We have structured this paper as follows. After briefly describing the minimal plateau inflationary model in section 2, we have briefly reviewed the parametric resonance phenomenon

in the early stage of reheating in section 3. In section 4 we have studied the analytic behavior of parametric resonance with the help of instability chart associated with the Mathieu/Hill type differential equations. In sections 5 and 6 we have presented the results of the lattice simulation. The perturbative reheating and CMB constrains on reheating phase has been described in section 6.4. Finally we conclude in section 7.

We will consider  $\hbar = c = 1$  unless otherwise stated. We have denoted  $m_p(= 1/\sqrt{G})$  as the Planck constant and  $M_p(= 1/\sqrt{8\pi G})$  as the reduced Planck constant. We will take the usual Friedmann-Leimatre-Roberson-Walker (FLRW) metric as our background metric  $ds^2 = dt^2 - a^2(t)(dx^2 + dy^2 + dz^2)$  for deriving our equations. With  $a(t)$  is the scale factor and  $t$  represents the cosmic time.

## 2 A Brief Introduction to the Minimal Inflation Model

In this section we will briefly introduce the minimal plateau inflationary model and its characteristics introduced in[15]. We have already explained in our previous paper, considering a simple power-law potential  $\phi^n$ , we can obtain our general class of non-polynomial form of the potential given as

$$V(\phi) = \frac{\lambda m^{4-n} \phi^n}{1 + \left(\frac{\phi}{\phi_*}\right)^n} \quad (2.1)$$

either by using conformal transformation in certain class of non-minimal scalar-tensor theory, or from the supergravity construction. The scale  $\phi_*$  can be identified with the non-minimal coupling in scalar-tensor theory, and inflationary energy scale in the supergravity potential. We take  $\lambda = 1$  for  $n \neq 4$  and the values of  $\lambda$  or,  $m$  is fixed from WMAP normalization. The inflationary predictions of this model has been studied extensively in the original work, here we present the  $n_s$  and  $r$  plot in fig.(1) on the latest Planck data[16]. After introducing the scalar potential, next we will introduce the parametric resonance after the end of inflation.

## 3 Preheating: Parametric resonance

### 3.0.1 Parametric resonance

In this section we briefly describe the method of identifying the parameter space within which parametric resonance occurs. It is the phenomena of exponential growth of a dynamical field coupled with an oscillating background in certain range of coupling and momentum. The fields under consideration could be the fluctuations of the inflaton or any other daughter field or both, which will see the homogeneous oscillating background inflaton for the present case. The daughter field coupled with the inflaton could be any other scalar field or usual standard model particles(usually bosons<sup>1</sup>). In order to understand the basic mechanism, one considers the following interaction Lagrangian for the inflaton ( $\phi$ ) and another scalar field ( $\chi$ ),

$$\mathcal{L}_\chi = \mathcal{L}_\phi + \frac{1}{2} \partial_\mu \chi \partial^\mu \chi - \frac{1}{2} m_\chi^2 \chi^2 - \frac{1}{2} g^2 \phi^2 \chi^2. \quad (3.1)$$

---

<sup>1</sup>the presence of bosons are important for parametric resonance, for preheating with fermions see, P. B. Greene and L. Kofman Phys. Lett B 448, 6 1999. [arXiv:hep-ph/9807339], P. B. Greene and L. Kofman Phys. Rev. D 62, 123516 2000. [arXiv:hep-ph/0003018]. we will here only consider the bosonic case

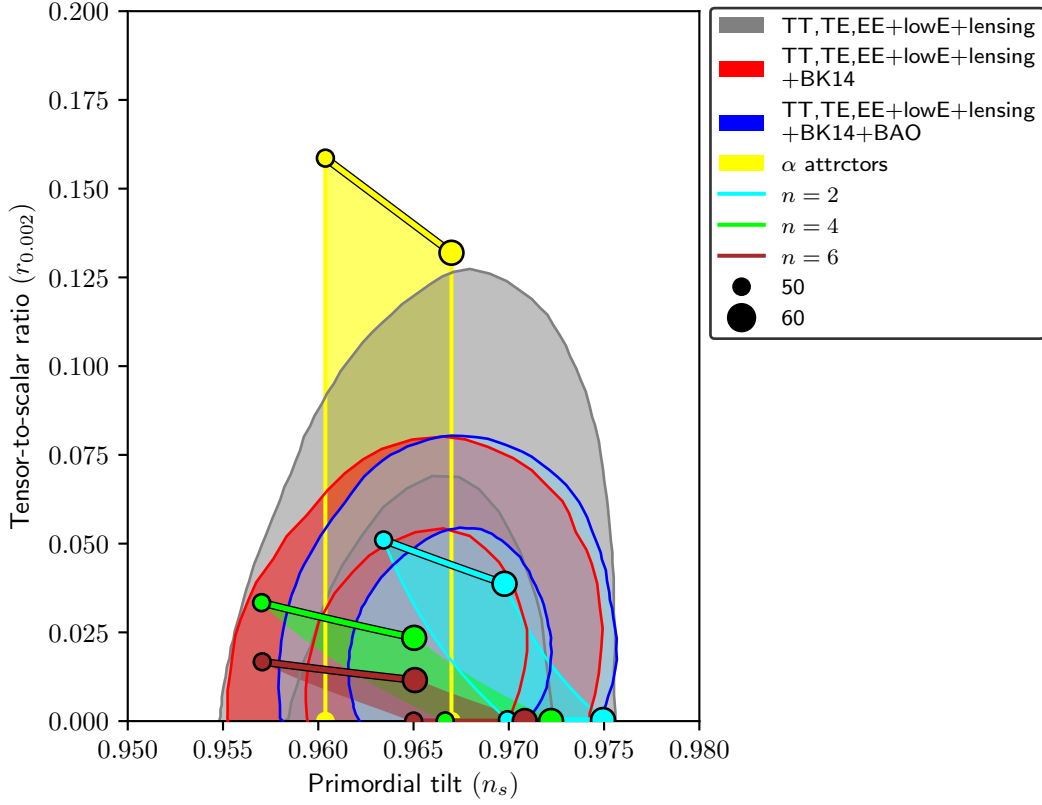


**Figure 1.** The  $n_s$  and  $r$  plot of the model on the marginalized joint 68% and 95% CL regions for  $n_s$  and  $r$  at  $k = 0.002 Mpc^{-1}$  from Planck alone and in combination with BK14 or BK14 plus BAO data. Dotted line corresponds to  $\phi_* = 10M_p$  and the solid line is for  $\phi_* = 0.1M_p$

Where,  $m_\chi$  is the mass of the  $\chi$  particle. The matter field  $\chi$  satisfies the following equation:

$$\ddot{\chi} + 3H\dot{\chi} - \frac{1}{a^2}\nabla^2\chi + (m_\chi^2 + g^2\phi^2)\theta = 0. \quad (3.2)$$

Decomposing the scalar field into its Fourier components,

$$\chi(t, x) = \int \frac{d^3\mathbf{k}}{(2\pi)^{2/3}} [a_{\mathbf{k}} \chi_k(t) e^{i\mathbf{k}\cdot\mathbf{x}} + h.c.], \quad (3.3)$$

the mode equation for  $\chi_k(t)$  then takes the following form

$$\ddot{\chi}_k + 3H\dot{\chi}_k + \left( \frac{k^2}{a^2} + m_\chi^2 + g^2\phi^2 \right) \chi_k = 0. \quad (3.4)$$

The associated number density of the particle with momentum  $k$  is given by [24]

$$n_k = \frac{\omega_k}{2} \left( \frac{|\dot{\chi}_k|^2}{\omega_k^2} + |\chi_k|^2 \right) - \frac{1}{2} \quad (3.5)$$

Where,  $\omega_k^2 = k^2 + a^2 m_\chi^2$ . The theory of parametric resonance has been studied extensively in the literature for simple potentials viz the power-law chaotic potentials [22, 25]. However for

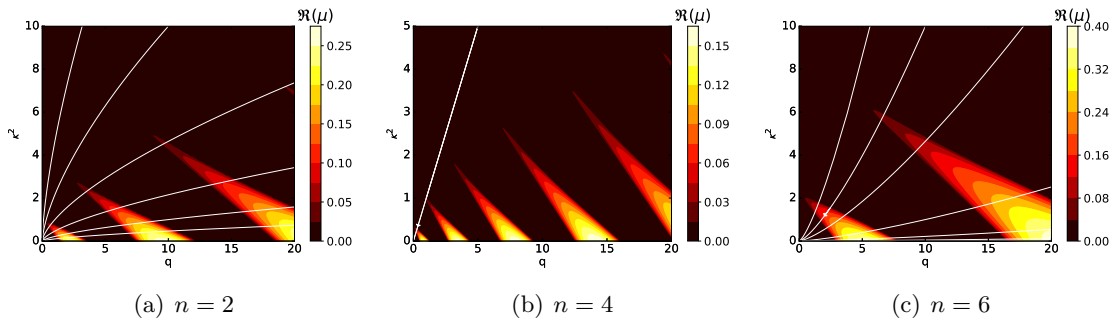


**Figure 2.** Instability regions for the models

the potentials of the form under consideration we need to solve the aforementioned equations numerically. Before describing the numerical results, we will analyze the resonance structure analytically by the studying the stability-instability diagram of the above equation with the well known method of Floquet analysis.

#### 4 Stability-Instability chart: Analytic Treatment

The instability of a mode is intimately tied with the violation of adiabatic condition that controls the particle production measured in terms of its growth over time. However this growth of a mode depends upon the coupling parameter and the value of the momentum. The exponential growth of a mode function depending upon the parameter values is termed as parametric resonance. To study this parametric resonance with the help of Mathieu/Hill equation we first do the following re-scaling  $X_k(t) \equiv a^{3/2}(t)\chi_k(t)$  to re-scale eq.(3.4) as

$$\ddot{X}_k + \omega_k^2 X_k = 0, \quad (4.1)$$

where

$$\omega_k^2 \equiv \frac{k^2}{a^2} + g^2 \phi^2(t) + \Delta, \quad \Delta \equiv -\frac{3}{4}(3H^2 + 2H). \quad (4.2)$$

During preheating, we will set  $\Delta = 0$ . To study the resonance phenomenon in the context of Floquet theory[36, 37], we will first ignore the expansion of the universe. Then eq.(4.2) can be identified as a form of Hill's differential equation

$$X_k'' + (\kappa + q\varphi^2(t)) X_k = 0, \quad (4.3)$$

with  $a = 1$  for no expansion, the coefficients  $\kappa$  and  $q$  given by  $\kappa = k^2/a^2$  and  $q = (g^2\Phi^2)/\mathcal{B}^2$  are time-independent. The time will be measured in unit of  $\mathcal{B}$  which will be model dependent. The homogeneous oscillatory background solution has been written as  $\phi(t) = \Phi\varphi(t)$ . In reality, the amplitude is also decaying with time i.e.,  $\Phi \equiv \Phi(t)$ . However, without expansion, we can take it to be constant. We will introduce the time dependence quantitatively later. The solution of the eq.(4.3) is of the form  $X_k \propto \exp(\mu_k t)$ . Where  $\mu_k$  is known as the Floquet exponent in the field of differential equations that set the nature of the solution. If  $\Re(\mu_{\kappa,q}) > 0$  for certain values of the parameters  $(\kappa, q)$ , the solution shows exponential growth which is identified as the particle production. The contours of  $\Re(\mu_{\kappa,q}) = 0$  in the  $(\kappa, q)$  plane, known as the instability

bands, help us to understand qualitatively the region of parameter space as well as the strength of the resonance during preheating. In figs.(2), we present the stability-instability chart for three different values of  $n = (2, 4, 6)$  for  $\phi_* = 10M_p$ . The shaded regions are the instability regions while the color-code value shows the strength of resonance. The effect of decreasing  $\phi_*$  for a particular  $n$ (not shown in the figure) is to shift the instability regions towards higher values of  $q$ . This is expected as decreasing  $\phi_*$  will result in reducing the initial amplitude of inflation field as the inflation becomes increasing sub-Planckian. Hence, we will naturally need a higher value of the coupling constant  $g$  to get the resonance. Also for a particular  $q$ (or,  $g$ ), decreasing  $\phi_*$  will lead to resonance only for the higher momentum modes. We will describe other important effects of the scale on preheating and thermalization as we go along. Till now, we have ignored the effect of expansion on the resonance phenomena. A striking difference between the parametric resonance in an expanding universe with the normal resonance is that the parameters  $(\kappa, q)$  in an expanding universe are not constants. They depend on time via the scale factor and the time-dependent amplitude  $\Phi(t)$  of the inflaton oscillation. As a result of the expanding universe all the momentum modes will be red-shifted while the back reaction of produced particles will eventually shut-down the resonance. Nonetheless, we may incorporate the effect of expansion in the instability analysis by noting including the fact that the amplitude of the inflaton oscillation will decay as  $\Phi \propto a^{-6/(n+2)}$ . Hence, a particular mode residing in an instability band in an expanding universe will not have indefinite growth rather it will travel through different instability and stability regions(when the solution is oscillatory indicating an absence of particle production) with time. The white flow-lines with the arrow direction shows the trajectory of a mode through different bands. Once we have the qualitative behavior of band structure, we are now in a position to understand the non-linear evolution.

## 5 Preheating: Lattice Simulation

The energy density of the universe just after the inflation is in the form of homogeneous inflaton field. This energy starts decaying into fluctuations of the inflaton and other fields at the onset of preheating. The initial stage of preheating is marked by exponential growth of decay product due to resonance. This highly non-linear and non-thermal production of inflaton and daughter particles continue until the back-reaction effects render the resonant production inefficient. Depending on the value of the resonance parameter  $q$  defined above, the preheating phase is usually classified into two regions: (i) For  $q < 1$ , the resonance is inefficient. We can treat the equations analytically in this ‘narrow-resonance’ regime. (ii) However, for broad parametric regime with  $q \gg 1$  the system is highly non-linear and we have to resort to numerical analysis. Also, the effects of back-reaction can be incorporated numerically. The numerical study of preheating will be done with the help of  $(3 + 1)d$  lattice simulation code namely the heavy-duty LATTICEASY[38] and its parallelized version CLUSTEREASY[39]. Below we will describe the model and equations to be solved in the code on a lattice .

### 5.1 The Model and equations

To implement the model in the lattice the inflaton potential has been slightly modified by dividing the factor  $n$  as:

$$V(\phi) = \frac{1}{n} \frac{\lambda m^{4-n} \phi^n}{\left[1 + \left(\frac{\phi}{\phi_*}\right)^n\right]} \quad (5.1)$$

The inflationary dynamics of this models has been describes in details in [15] while the perturbative reheating and production of dark matter has been considered in [17]. It must be mentioned that for large values of the scale  $\phi_* \gg M_p$  our model reduces to usual power law chaotic model. All these simple power law models are already ruled out considering the CMB observation. However, once we consider the non-polynomial modification of the power law such as ours, models turned out to be observationally viable for a large parameter space fig. 1. Given a specific model of inflation, we need to further model the interaction of inflation with the daughter particle for preheating to happen. We have already specified our interaction Lagrangian as

$$\mathcal{L}_{int} = -\frac{1}{2}g^2\phi^2\chi^2 \quad (5.2)$$

It has been noted that this four-legged interaction term will be dominant over the three-legged interaction viz  $g^2\sigma\phi\chi^2$  for the initial stages of preheating when the amplitude of the homogeneous inflaton oscillation is large. This interaction does not lead to any tree level decay of the inflaton and particle production will solely due to non-perturbatives processes. The four-legged interaction is usually not able to complete the decay of inflaton for general chaotic inflationary scenario[40]. Therefore, after the preheating three-legged interaction will be dominating in the perturbative decay process and may complete the reheating dynamics. In this work we will exclusively consider the aforementioned interaction for the preheating stage. At the end we will discuss about the perturbative reheating and connection with CMB. Nevertheless, the full potential for our lattice simulation is

$$V(\phi, \chi) = \frac{1}{n} \frac{\lambda m^{4-n} \phi^n}{\left[1 + \left(\frac{\phi}{\phi_*}\right)^n\right]} + \frac{1}{2}g^2\phi^2\chi^2. \quad (5.3)$$

With this potential LATTICEEASY will solve the following classical scalar field equations

$$\ddot{\phi} + 3H\dot{\phi} - \frac{1}{a^2}\nabla^2\phi + \frac{\partial}{\partial\phi}V(\phi, \chi) = 0, \quad (5.4)$$

$$\ddot{\chi} + 3H\dot{\chi} - \frac{1}{a^2}\nabla^2\chi + \frac{\partial}{\partial\chi}V(\phi, \chi) = 0. \quad (5.5)$$

While the Hubble parameter  $H$  is calculated self-consistently from the Friedmann equation. Denoting the preheating fields as a generic symbol  $f(t, \vec{x})$  and its Fourier transform as  $f_k(t)$ , the (comoving) occupation number of particles are given by[38, 40]

$$n_k(t) \equiv \frac{1}{\omega_k}|\dot{f}_k|^2 + \frac{\omega_k}{2}|f_k|^2, \quad \text{with,} \quad \omega_k \equiv \sqrt{k^2 + m_{eff}^2}, \quad \text{and,} \quad m_{eff}^2 \equiv \frac{\partial^2 V}{\partial f^2} \quad (5.6)$$

The evolution of various energy components such as kinetic, gradient and interaction part contain important information about the thermalization process and building of inhomogeneity. We will study in detail the evolution of those individual components defined below

$$\rho \equiv E_t = (E_\phi^K + E_\chi^K + E_\phi^G + E_\chi^G + E_\phi^P + E_{\phi\leftrightarrow\chi}^I) \quad (5.7)$$

Where,

$$E_\phi^K = \frac{1}{2}\dot{\phi}^2; \quad E_\chi^K = \frac{1}{2}\dot{\chi}^2; \quad (5.8)$$

$$E_\phi^G = \frac{1}{2a^2}(\nabla\phi)^2, \quad E_\chi^G = \frac{1}{2a^2}(\nabla\chi)^2; \quad (5.9)$$

$$E_\phi^P = V(\phi), \quad E_{\phi\leftrightarrow\chi}^I = \frac{1}{2}g^2\phi^2\chi^2. \quad (5.10)$$

Where, the subscript ( $K, G, P, I$ ) stand for kinetic, gradient, potential and interaction component of the total energy respectively. However, for evolution of the scale factor it is the total energy density  $\rho$  that plays the important role. The energy total energy density may be expressed as

$$\rho \approx \frac{1}{(2\pi)^3 a^4} \int d^3k \omega_k n_k, \quad (5.11)$$

and the total (comoving) number density of the  $f$  field is expressed as

$$n_f(t) \equiv \frac{1}{2\pi^2} \int d^3k n_k(t). \quad (5.12)$$

In next section we will consider different set of our model parameters ( $n, \phi_*$ ) and try to compare their outcomes in terms of time evolution of various non-equilibrium observables.

## 6 Analysis and Results

We have performed the lattice simulations in  $3 + 1$  dimension with a  $256^3$  grid. We have measured time with a dimensionless parameter  $z = \mathcal{B}t$  with  $\mathcal{B} = \phi_0^{n/2-1} \sqrt{\lambda m^{4-n}}$  ( $\phi_0$  being the initial inflaton amplitude) set the natural time scale of the systems. Depending upon the run time for simulation taken we sometimes used  $128^3$  or  $512^3$  lattices for convenience. Where as in the case of defining the potentials we take  $\lambda = 1$  when  $n = 4$ . The vales of  $m$  and  $\lambda$  are fixed from WMAP normalization.

### 6.1 The back-reaction and the emergence of non-linearity

The preheating phase in general is episodic with three distinct phases. Before making a quantitative description of these phases for different values of  $n$  and  $\phi_*$ , let us first describe the general characteristics of the phases. The first phase of preheating is marked by the linear growth of produced field(s) via parametric resonance. The comoving amplitude of the inflaton field remains almost constant throughout this phase while most of the energy of the system is contained in the inflaton field oscillating mostly in the form of kinetic and potential energies. While all other energies are sub-dominant. The characteristic scale marking the end of this phase will be denoted by the instant  $z_{br}$  where ‘br’ stands for back-reaction. In practice, we will measure  $z_{br}$  as an instant when the comoving inflaton amplitude drops to 95% of its initial value. The second phase is the non-linear regime when the back-reaction of the produced field quanta became appreciable on the dynamics of the inflaton field. As a result, the comoving amplitude of the field starts decreasing appreciably. Inflaton kinetic and potential energies start to decrease resulting in the increase of other energy components. The gradient energy of the inflaton field which represents the growth of the inhomogeneities will also start to increase. This phase ends when the inflaton decay stops. We will denote the end of this phase as  $z_{dec}$ . Where ‘dec’ represents the instant when the inflaton field decouples form the produced field and enters into a stationary regime.

Another interesting aspect of preheating is observed by observing the virialization of the system. The inflaton with a potential  $V(\phi) \propto \phi^n$  and the produced field satisfy the following

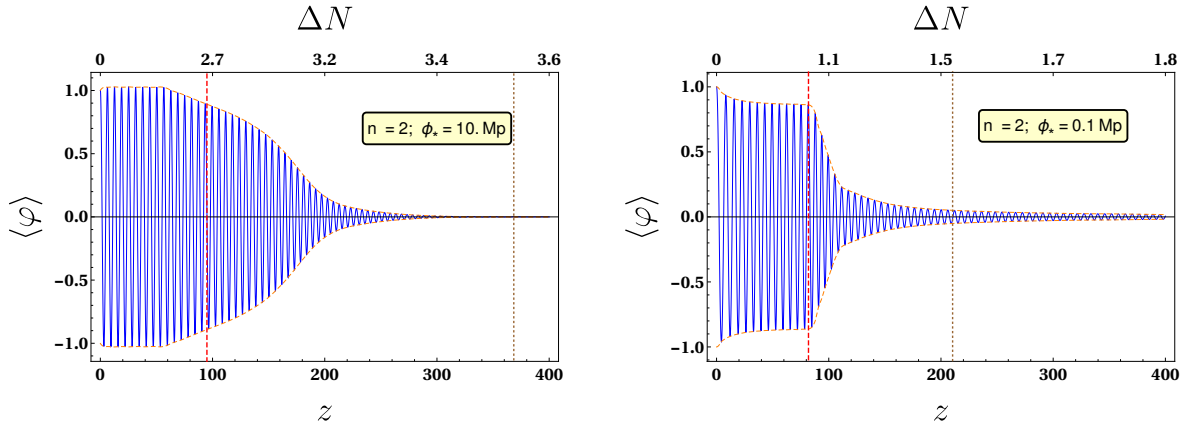


**Figure 3.** Evolution of volume averaged comoving inflation amplitude  $\varphi = (a/a_i)^{3/2}(\phi/\phi_0)$  not zero mode! for the model potential  $n = 2$  for  $\phi_* = 10M_p$  and  $0.1M_p$ . The red dashed line shows the instant of back-reaction initiation while the brown dotted line is for the instant of decoupling.

virialization relation.

$$\frac{1}{2} \langle \dot{\phi}^2 \rangle = \frac{1}{2} \left\langle \left( \frac{\nabla \phi}{a} \right)^2 \right\rangle + \frac{n}{2} \langle V(\phi) \rangle + \frac{1}{2} \langle g^2 \phi^2 \chi^2 \rangle \quad (6.1)$$

$$\frac{1}{2} \langle \dot{\chi}^2 \rangle = \frac{1}{2} \left\langle \left( \frac{\nabla \chi}{a} \right)^2 \right\rangle + \frac{1}{2} \langle g^2 \phi^2 \chi^2 \rangle \quad (6.2)$$

Where the average is over space and time. We will discuss the virialization of each system separately below. Through out our study we will compare models under consideration for mainly two different value of  $\phi^*$ .

### 6.1.1 General description of figures and results

Before we discuss in detail specific models and their behavior in this subsection let us describe various figures and the general behaviors of the preheating dynamics. For every model we have plotted four sets of figures. In the set of figs.3,5,7 we have plotted the evolution of the inflaton field with time scale  $z$  and e-folding number  $\Delta N$ . For a given  $n$  we have chosen a particular value of  $g$  with different inflationary scale parameter  $\phi_*$ . What we observed is that with decreasing  $\phi^*$  the duration of non-perturbative reheating process quantified by  $\Delta N$  is also decreasing. This essentially means the decay of inflaton will be efficient for higher lower  $\phi^*$ . We have already mentioned in the introduction, from the figures we can clearly see three stages of preheating. In the beginning the inflaton amplitude remains almost constant which means energy transferred from  $\phi$  to  $\chi$  will very small and it dominated by parametric resonance. The next stage is the most important phase of the entire non-perturbative regime when the system become highly turbulent because of cascade and inverse cascade of energy between two the species of particles. Energy transfer from inflaton to reheating field becomes exponentially enhanced. This is the phase when equation of state of both the fields also quickly changes from their initial background value to almost saturation value before the system could reach thermal equilibrium. Once the thermal equilibrium is achieved, in the third phase inflaton amplitude settles down again to a constant value without further decay. In an another set of figs.4,6,8, we plotted the evolution of various components of the total energy of the individual fields.

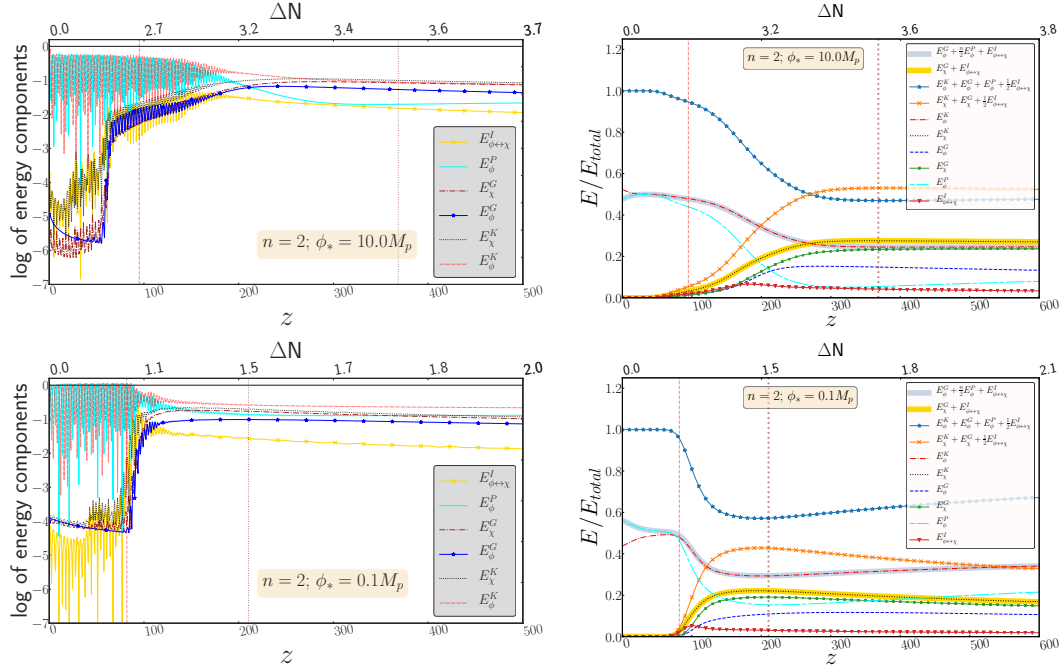


**Figure 4.** The variation of energy components normalized by the initial energy with time and the e-folding number is shown. The plot in the right is oscillation average.

From this we can understand how the inhomogeneity evolves and disappears during this non-linear process. This seems to be a generic phenomena that during the parametric resonance dominated phase most of the energy will contained in the homogeneous mode of inflation. Once the back reaction sets in, the inhomogeneity starts to grow and again becomes What we have observed is that for  $n = 2$  the complete thermalization takes longer time compared with the other models where thermalization happens for  $\Delta N \leq 4.5$ . Even more importantly, for all the cases, only 50% of the total co-moving inflaton energy density has been transferred into the reheating field  $\chi$ . In the figs.figs. 9 to 11, we have plotted the time evolution of an important reheating parameter called equation of state  $w$ . It turned out that for  $n > 2$ , after the end of preheating each individual field attends the equation of state  $w = 1/3$  for all different model parameters irrespective of the form of the potential. With this general discussion, in the subsequent sections we will discuss in detail each model for different parameter values and their behavior. For each inflationary model under consideration corresponding to a particular value of  $n$ , we compare the results considering a particular value of  $g$  and two set of values for  $\phi_*$ .

### 6.1.2 $n = 2$

Since we will be considering different inflationary models where different kind of parametrization will needed for the our lattice simulation. We will describe those in detail for energy model. For  $n = 2$  model, using the default re-scaling scheme of LATTICEASY, we define the following quantities that will be used for simulation

$$\varphi \equiv \frac{\phi}{\phi_0} a^{\frac{3}{2}}, \quad X \equiv \frac{\chi}{\phi_0} a^{\frac{3}{2}}, \quad z \equiv mt, \quad \vec{z} \equiv m\vec{x}. \quad (6.3)$$

**Table 1.** Fractions of energy components at  $z = z_{br}$  for  $n = 2$ 

$\phi_*(M_p)$	$\frac{E_\phi^K}{E_T}$	$\frac{E_\phi^P}{E_T}$	$\frac{E_\chi^K}{E_T}$	$\frac{E_{\phi\leftrightarrow\chi}^I}{E_T}$	$\frac{E_\phi^T}{E_T}$	$\frac{E_\chi^T}{E_T}$
10	48.0%	44.0%	3.0%	2.0%	95.0%	5.0%
0.1	48.0%	46.3%	2.7%	2.1%	95.0%	5.0%

**Table 2.** Fractions of energy components at  $z = z_{dec}$  for  $n = 2$ 

$\phi_*(M_p)$	$\frac{E_\phi^K}{E_T}$	$\frac{E_\phi^P}{E_T}$	$\frac{E_\phi^G}{E_T}$	$\frac{E_\chi^K}{E_T}$	$\frac{E_\chi^G}{E_T}$	$\frac{E_{\phi\leftrightarrow\chi}^I}{E_T}$	$\frac{E_\phi^T}{E_T}$	$\frac{E_\chi^T}{E_T}$
10	24.5%	5.5%	14.6%	27.6%	23.4%	4.1%	47.0%	53.0%
0.1	29.4%	15.4%	11.0%	22.2%	19.1%	3.1%	57.2%	42.7%

where  $x^\mu \equiv (t, \vec{x})$  is the cosmic time and comoving coordinate. The field equations described in eq. (5.4) now reduces to

$$\varphi'' - \frac{1}{a^2} \nabla^2 \varphi - \left[ \frac{3}{4} \left( \frac{a'}{a} \right)^2 - \frac{3}{2} \frac{a''}{a} \right] \varphi + \frac{\mathcal{Q}}{a^3} \varphi X^2 + \frac{\partial}{\partial \varphi} V(\varphi) = 0 \quad (6.4)$$

$$X'' - \frac{1}{a^2} \nabla^2 X - \left[ \frac{3}{4} \left( \frac{a'}{a} \right)^2 - \frac{3}{2} \frac{a''}{a} \right] X + \frac{\mathcal{Q}}{a^3} \varphi^2 X = 0. \quad (6.5)$$

Where  $prime(t)$  denotes derivative with respect to  $z$  and  $\mathcal{Q}$  is the resonance parameter defined as

$$\mathcal{Q} \equiv \frac{g^2}{m^2} \phi_0^2$$

We chose the two values of  $\phi_* = (10M_p, 0.1M_p)$ . To facilitate comparison with previous works, in all our lattice simulation we have set  $M_p = 1$ . Now from the PLANCK normalization the value of the scale  $m = (1.38 \times 10^{-6}, 9.38 \times 10^{-6})$  in unit of  $M_p$ . We have started our simulation when  $\varphi'(z_0) = 0$  with the initial field values at  $(0.191, 0.0157)$ . The coupling parameter for both values of  $\phi_*$  is chosen as  $g^2 = 2.2 \times 10^{-5}$ . The evolution of the inflaton zero mode for two values of  $\phi_*$  has been shown in fig(3). The back-reaction of the  $\chi$  field starts to play role within  $\Delta N_{br} \sim (2.7, 1)$  for  $\phi_* = (10M_p, 0.1M_p)$ . It is evident that the duration of parametric resonance phase decreases with decreasing  $\phi_*$ . In the fig(4) left two panel describes the evolution of every individual energy component of inflaton and reheating field with respect to  $z$ . Where as in the right panels it is their time average. In order to quantitatively understand, the fractions of different energy components have been tabulated. From tab.(1), we can clearly see that during the phase when parametric resonance is the dominant channel for the decay of inflaton, irrespective of  $\phi_*$  value, only 5% of the total energy component is getting transferred into the reheating field. However most efficient transfer of energy occurs after the onset of back-reaction till the stationary phase is achieved with complete thermalization at around  $\Delta N_{dec} \sim (3.5, 1.5)$  for the two values of  $\phi_*$ . After the end of this back-reaction dominated phase at  $z = z_{dec}$ , all individual energy component freezes out to a constant value given in the table(2). At this point let us bring to our reader's notice an important characteristic feature in non-linear regime of thermalization is that during this phase the inhomogeneity starts to grow rapidly for both the field and then freeze out

after the stationary phase. It would be interesting to understand the fact that as we decrease  $\phi_*$  the growth of inhomogeneity is less. Therefore, for smaller value of  $\phi_*$  or in other for small scale inflation, local inhomogeneity during reheating will be suppressed and it can have interesting effect after the end of reheating. We will see in our subsequent discussions that this behavior of inhomogeneous evolution depending upon  $\phi_*$  will be similar for other models such as  $n = 4, 6$ . Analytic understanding of this phenomena could be interesting. As has been mentioned before, irrespective of the value of  $\phi_*$ , only 50% of the inflation energy density has been transferred to the reheating  $\chi$  field before non-perturbative production being completely stopped. Therefore, in order to complete the decay we need to perform perturbative decay separately to obtain the reheating temperature, that we will discuss in the end. For this process three leg interaction  $\phi\chi^2$  may be dominant. In our future publication we will consider both four and three leg interactions to examine decay process and thermalization.

In any case for  $n = 2$  we should emphasize the fact that our numerical simulation does not give the condition of equal energy distribution among the inflaton and daughter particle in the stationary phase. As mentioned earlier the equation of state of both the field does not become that of the radiation as opposed to other models  $n = 4, 6$  that will be discussed in the subsequent sections.

### 6.1.3 $n = 4$

For  $n = 4$  model we define the following dimensionless quantities that will be used for simulation

$$\varphi \equiv \frac{\phi}{\phi_0} a^{-1}, \quad X \equiv \frac{\chi}{\phi_0} a^{-1}, \quad z \equiv \phi_0 \sqrt{\lambda} t, \quad \vec{z} \equiv \phi_0 \sqrt{\lambda} \vec{x}. \quad (6.6)$$

where  $x^\mu \equiv (t, \vec{x})$  is the cosmic time and comoving coordinate. The field equations described in eq. (5.4) now reduces to

$$\varphi'' - \nabla^2 \varphi - \frac{a''}{a} \varphi + \mathcal{Q}_\varphi X^2 + \frac{\partial}{\partial \varphi} V(\varphi) = 0 \quad (6.7)$$

$$X'' - \nabla^2 X - \frac{a''}{a} X + \mathcal{Q}_\varphi^2 X = 0. \quad (6.8)$$

The resonance parameter is defined as

$$\mathcal{Q} \equiv \frac{g^2}{\lambda}$$

For this also we chose two values of  $\phi_* = (10M_p, 0.1M_p)$ . From PLANCK normalization the value of the dimensionless parameter  $\lambda$  turned out to be  $(4.2 \times 10^{-13}, 4.7 \times 10^{-8})$ . At the end of inflation the field values assumes  $(0.342M_p, 0.0177M_p)$ . The coupling parameter for both the run is chosen to be  $g^2 = 2.3 \times 10^{-5}$ . As we mentioned and also clearly seen from various plots, the qualitative behavior of decaying inflaton for this case is similar to that of  $n = 2$  model. From the figs.6 we see with the decreasing  $\phi_*$ , the decay of inflaton become efficient. After the initial linear regime, for this case the back-reaction sets in at around  $\Delta N_{br} = (3.2, 0.9)$  e-folding number while the subsequent stationary phase is achieved at  $\Delta N_{dec} = (4.7, 2.2)$ . The qualitative behavior of this model will be the same as  $n = 2$  case. However, from the table(4) it is important to see that in the stationary phase the total energy becomes equally distributed between the inflaton and the daughter field.

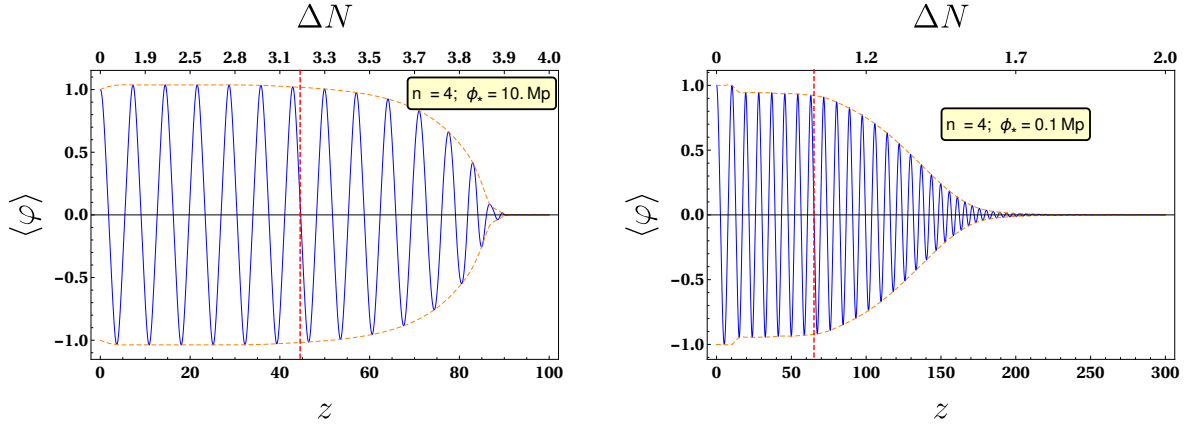


**Figure 5.** Evolution of volume averaged comoving inflation  $\varphi = (a/a_i)(\phi/\phi_0)$  amplitude for the model potential  $n = 4$  for  $\phi_* = 10M_p$  and  $0.1M_p$

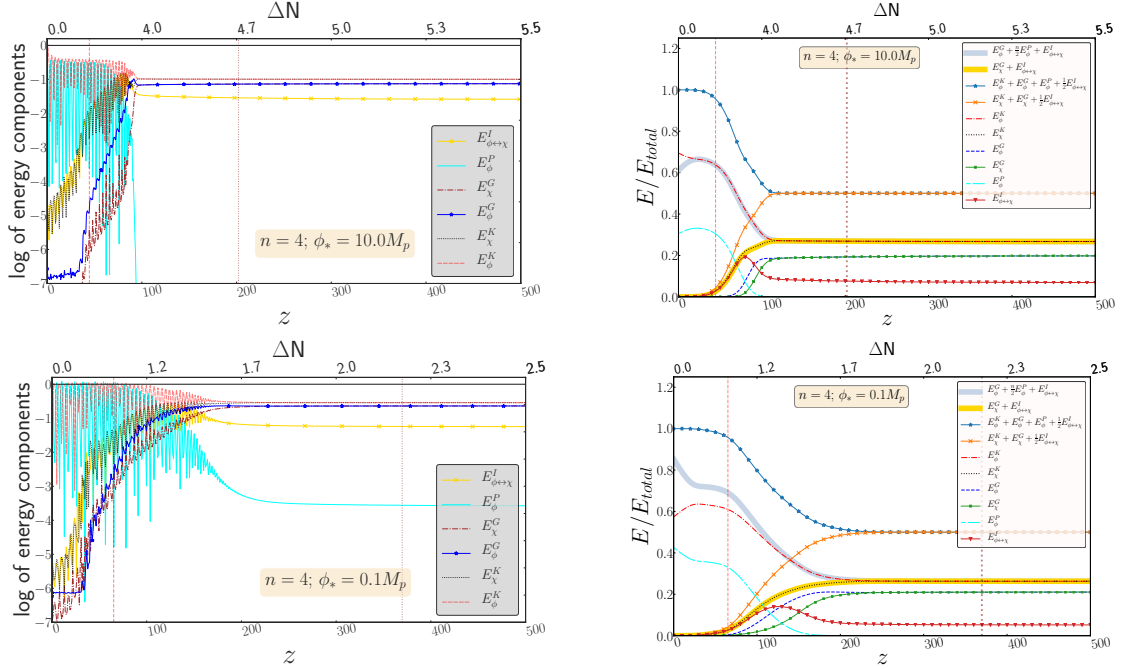


**Figure 6.** The variation of energy components with time and the e-folding number is shown.

#### 6.1.4 $n = 6$

For this model the re-scaled variables are defined as

$$\varphi \equiv \frac{\phi}{\phi_0} a^{\frac{3}{4}}, \quad X \equiv \frac{\chi}{\phi_0} a^{\frac{3}{4}}, \quad z \equiv \frac{\phi_0^2}{m} t, \quad \vec{z} \equiv \frac{\phi_0^2}{m} \vec{x}. \quad (6.9)$$

**Table 3.** Fractions of energy components at  $z = z_{br}$  for model  $n = 4$ 

$\phi_*(M_p)$	$\frac{E_\phi^K}{E_T}$	$\frac{E_\phi^P}{E_T}$	$\frac{E_\chi^K}{E_T}$	$\frac{E_{\phi\leftrightarrow\chi}^I}{E_T}$	$\frac{E_\phi^T}{E_T}$	$\frac{E_\chi^T}{E_T}$
10	62.6%	29.2%	4.5%	3.9%	93.8%	6.2%
0.1	63.7%	30.4%	3.0%	2.8%	95.0%	5%

**Table 4.** Fractions of energy components at  $z = z_{dec}$  for model  $n = 4$ 

$\phi_*(M_p)$	$\frac{E_\phi^K}{E_T}$	$\frac{E_\phi^P}{E_T}$	$\frac{E_\phi^G}{E_T}$	$\frac{E_\chi^K}{E_T}$	$\frac{E_\chi^G}{E_T}$	$\frac{E_{\phi\leftrightarrow\chi}^I}{E_T}$	$\frac{E_\phi^T}{E_T}$	$\frac{E_\chi^T}{E_T}$
10	26.9%	–	19.3%	27.0%	19.3%	7.6%	50.0%	50.0%
0.1	26.3%	0.2%	21.0%	26.3%	21.0%	5.2%	50.0%	50.0%

The field equations described in eq. (5.4) for  $n = 6$  reduces to

$$\varphi'' - a\nabla^2\varphi - \left[ \frac{3}{4} \frac{a''}{a} - \frac{3}{16} \left( \frac{a'}{a} \right)^2 \right] \varphi + \mathcal{Q} a^{\frac{3}{2}} \varphi X^2 + \frac{\partial}{\partial\varphi} V(\varphi) = 0 \quad (6.10)$$

$$X'' - a\nabla^2 X - \left[ \frac{3}{4} \frac{a''}{a} - \frac{3}{16} \left( \frac{a'}{a} \right)^2 \right] \varphi + \mathcal{Q} a^{\frac{3}{2}} \varphi^2 X = 0. \quad (6.11)$$

Where the resonance parameter turned out as

$$\mathcal{Q} \equiv \frac{g^2 m^2}{\phi_0^2}$$

As opposed to the other two models  $n = 2, 4$ , for the this case we chose  $\phi_* = (1M_p, 0.5M_p)$ , and consequently the lattice input parameter turned out to be  $g^2 m^2 = (200, 9)$  so that the simulation time is within our reach. It has been found that the model with  $n = 6$  takes the longer time for simulation which further increases with increasing value of the coupling parameter  $g^2$ . With our present computational resource as well as for optimum run time, we are able to simulate for the values of the input parameter  $g^2 m^2 < 1000$ . The value of the scale  $m$  from WMAP normalization becomes  $(7.2 \times 10^{-8}, 3.2 \times 10^{-7})$  that will be our one set of input parameters. After the end of inflation the initial field values are taken to be  $(0.226, 0.138)$  and the coupling parameter for both  $\phi_*$  value is chosen as  $g^2 = 2.8 \times 10^{-7}$ . The simulation results show that the non-linear back-reaction regime starts at around  $\Delta N_{br} = (3.5, 3.0)$  and then finally the equilibrium condition is achieved at  $\Delta N_{dec} = (4.5, 3.8)$  for the two values of  $\phi_*$ . In this case too, the energy will be distributed equally to both inflaton and daughter field as opposed to  $n = 2$  case as seen in table(6).

## 6.2 Equation of state

The equation of state is one of the most important parameters to study during preheating. The equation of state in this context is defined as:

$$w = \frac{p}{\rho} = \frac{\frac{1}{2}\dot{\phi}^2 + \frac{1}{2}\dot{\chi}^2 - \frac{1}{3}\frac{(\nabla\phi)^2}{2a^2} - \frac{1}{3}\frac{(\nabla\chi)^2}{2a^2} - V(\phi, \chi)}{\frac{1}{2}\dot{\phi}^2 + \frac{1}{2}\dot{\chi}^2 + \frac{(\nabla\phi)^2}{2a^2} + \frac{(\nabla\chi)^2}{2a^2} + V(\phi, \chi)} \quad (6.12)$$

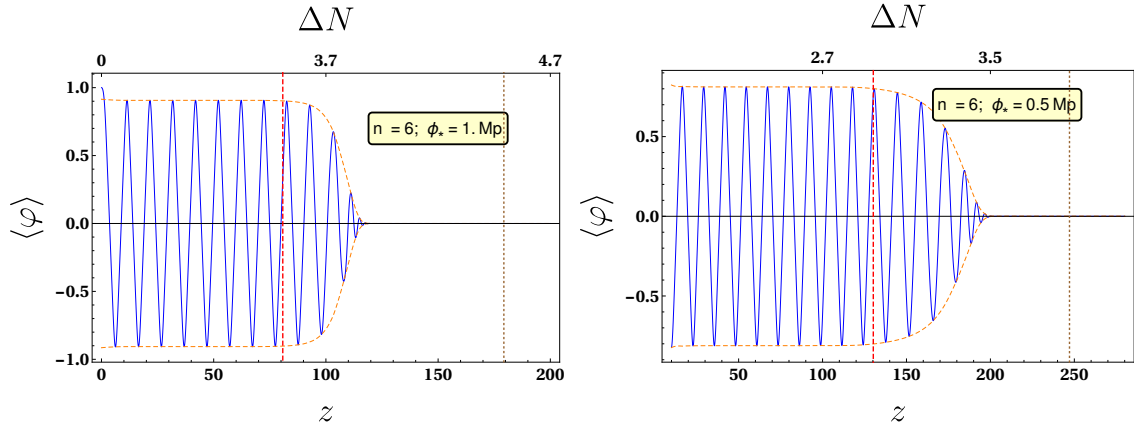


**Figure 7.** Evolution of volume averaged comoving inflation ( $\varphi = (a/a_i)^{3/4}(\phi/\phi_0)$ ) amplitude for the model potential  $n = 6$  for  $\phi_* = 10M_p$  and  $0.1M_p$

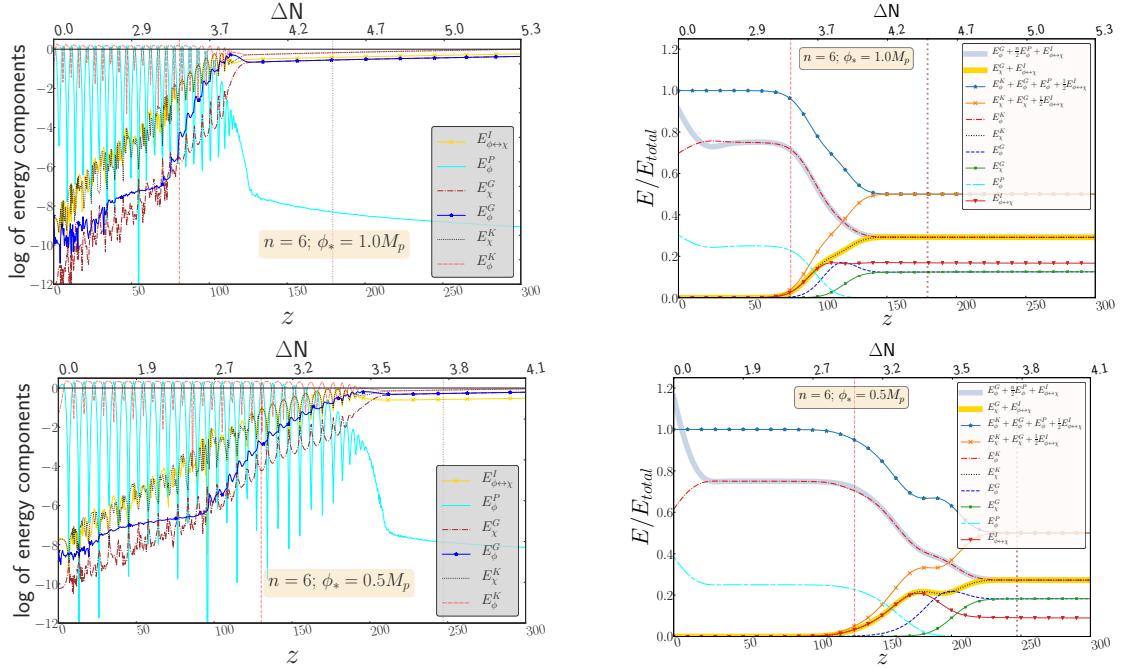


**Figure 8.** The variation of eos with time and the e-folding number is shown.

For homogeneous inflaton condensate oscillating in a potential  $V(\phi) \propto \phi^n$ , the equation state is given by [11]  $w = (n-2)/(n+2)$ . The inflaton initially oscillates with this equation of state till the other components of the total energy such as gradient, interaction energy became significant and resulting in fragmentation. Ignoring the interaction energy, and using the virial relations given in eq.6.2 the definition of  $w$  in 6.12 transforms into

$$w = \frac{1}{3} + \frac{(n-4)}{6} \frac{1}{\frac{n+2}{4} + \frac{\langle (\nabla\phi)^2/2a^2 \rangle}{\langle V(\phi) \rangle} + \frac{\langle (\nabla\chi)^2/2a^2 \rangle}{\langle V(\phi) \rangle} + \frac{3}{2} \frac{\langle V_I \rangle}{\langle V(\phi) \rangle}} \quad (6.13)$$

**Table 5.** Fractions of energy components at  $z = z_{br}$  for model  $n = 6$ 

$\phi_*(M_p)$	$\frac{E_\phi^K}{E_T}$	$\frac{E_\phi^P}{E_T}$	$\frac{E_X^K}{E_T}$	$\frac{E_X^G}{E_T}$	$\frac{E_{\phi\leftrightarrow X}^I}{E_T}$	$\frac{E_\phi^T}{E_T}$	$\frac{E_X^T}{E_T}$
1	71.5%	22.8%	2.7%	0.3%	2.7%	95.0%	5.0%
0.5	70.3%	22.7%	3.4%	0.2%	3.4%	95.0%	5.0%

**Table 6.** Fractions of energy components at  $z = z_{dec}$  for model  $n = 6$ 

$\phi_*(M_p)$	$\frac{E_\phi^K}{E_T}$	$\frac{E_\phi^G}{E_T}$	$\frac{E_X^K}{E_T}$	$\frac{E_X^G}{E_T}$	$\frac{E_{\phi\leftrightarrow X}^I}{E_T}$	$\frac{E_\phi^T}{E_T}$	$\frac{E_X^T}{E_T}$
1	29.2%	12.4%	29.2%	12.4%	16.8%	50.0%	50.1%
0.5	27.3%	18.2%	27.3%	18.2%	9.0%	50.0%	50.0%

Using the values of average energies of different components listed in tables 2, 4 and 6, we found that  $w \rightarrow 0.2$  for  $n = 2$  and  $w \rightarrow 1/3$  for  $n = 4$ , and 6 in the stationary phase. The results of the Simulation are plotted in figs. 9 to 11. We have plotted the instantaneous equation of state (brown curves) as well as the average value over a period of inflaton oscillation (red dashed curves). The green line shows the homogeneous Inflation equation of state. The features we note from these figs for different models are

- (i) For  $n = 2$  models, the equation of state make a transition from  $w = 0$  to  $w \sim 0.2 - 0.3$  within a few e-folding number. However, the equation of state never reaches the radiation like equation of state ( $w = 1/3$ ). This behavior has also been noted in [41] for the  $m^2\phi^2$  model. Similar behavior is expected as our model boils down to usual power law potential near the minimum at  $\phi = 0$ . We also observed that reducing the scale  $\phi_*$  does not improve the scenario except duration of preheating phase. We have found that with longer simulation equation of state starts decreasing after reaching a maximum  $w \sim 0.3$  and finally settles to  $w \rightarrow 0.1$ . The reason for this behavior is that for  $n = 2$  model, which is identical to  $m^2\phi^2$  around the minimum, the massive inflaton component although may remain under-abundant during preheating eventually rise up to dominate after the inflation decay ceases. It has also been found [41] that  $w(t)$  depends non-monotonically on the resonance parameter  $q$  (or alternatively on the coupling  $g^2$ ) for higher value of  $\phi_*$ . However it has been found that increasing  $g^2$  will not help us reaching the radiation domination as shown in figure (12). However, interesting observation can be made on the dependence of  $\phi_*$ . For lower value of  $\phi_* = 0.1$  the equation of state  $w$  changes almost instantaneously from zero to its saturation value before the system could reach the thermal equilibrium and apparently it also behaves monotonically with respect to coupling parameter  $g^2$ . Therefore, lowering the value of  $\phi_*$  makes the intermediate or the turbulent phase more efficient.
- (ii) For  $n = 4$  model, the homogeneous condensate itself oscillates with  $w = 1/3$  at the onset of preheating. The simulation results shows that it retains the radiation like equation of state throughout the simulation period. Decreasing  $\phi_*$  have the same qualitative behavior, with an important difference compared to  $n = 2$  model is that intermediate or turbulent regime occurs for longer time. Therefore the evolution of  $w(t)$  do not provide any additional information about the thermalization process in this case.

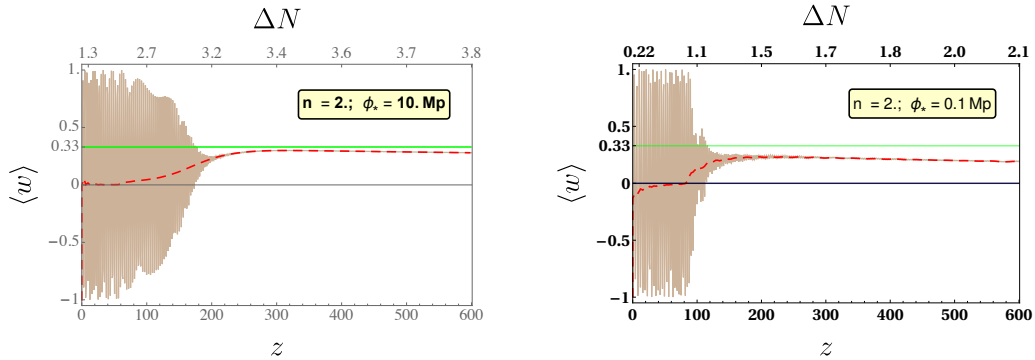


**Figure 9.** The variation of equation of state with time as well as the effect of the scale  $\phi_*$  is evident. The solid blue lines are the instantaneous value of the equation of state while the red dotted line is the averaged value over a period of inflaton oscillation. Time is measured in unit of their respective scale  $m$  hence to facilitate a comparison between different models, the e-folding number is shown in the upper panel.

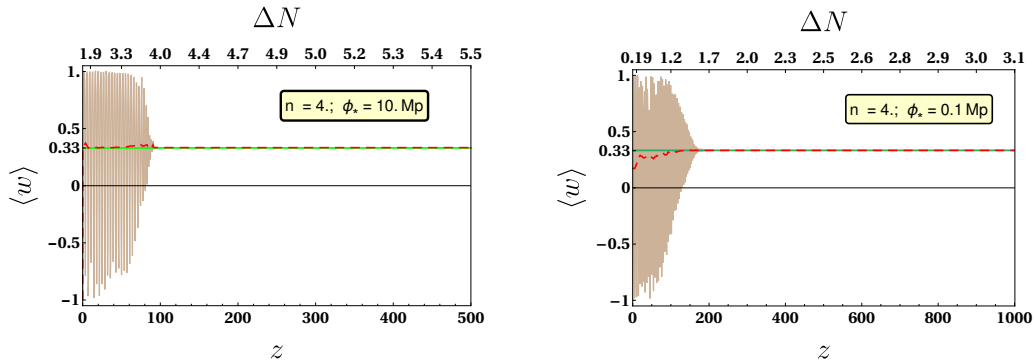


**Figure 10.** The variation of equation of state with time as well as the effect of the scale  $\phi_*$  is evident. The solid blue lines are the instantaneous value of the equation of state while the red dotted line is the averaged value over a period of inflaton oscillation. Time is measured in unit of their respective scale  $m$  hence to facilitate a comparison between different models, the e-folding number is shown in the upper panel.

- (iii) In the case of model with  $n = 6$ , the homogeneous condensate has equation of state  $w = 1/2$ . For this case the equation of state makes a transition from  $w \rightarrow 1/3$  for all value of  $\phi_*$ . However, important point to notice that the transition time decreases with the increasing value of  $\phi_*$  which is opposite to that of  $n = 2$  case.

### 6.3 Occupation Numbers

Evolution of occupation number for different modes is an another important parameter that contains important information about the microscopic mechanism of the preheating as well as the details of thermalization process. In general the occupation number will be well defined if the interaction energy is negligibly small. It is apparent from figs. 4, 6 and 8 that during the whole preheating period, the interaction energy is dominated only for a very brief period of time right after the initial parametric regime where re-scattering effect is important. Therefore, the occupation number ( $n_k^\phi, n_k^X$ ) of the fields are always well defined except for this small interval. Following [39, 41], we, therefore, can understand the thermalization process across all possible modes by considering the Rayleigh-Jeans spectrum defined by the product  $n_k \omega_k \simeq T$  in the large occupation number limit which is generally true during preheating. The

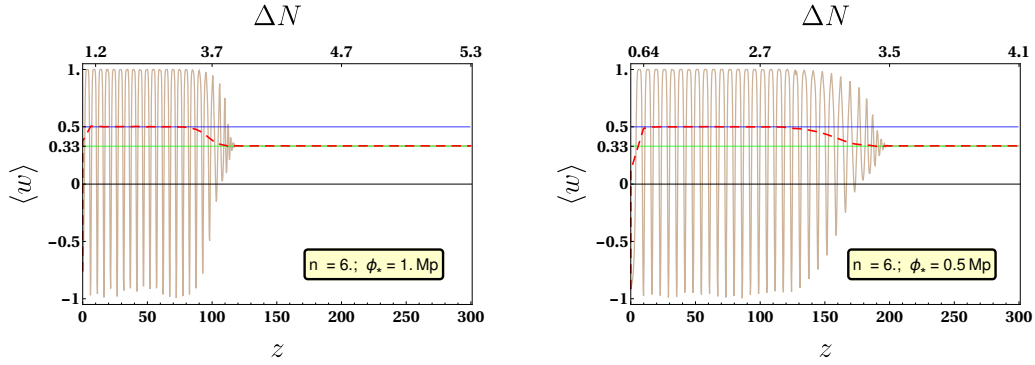


**Figure 11.** The variation of equation of state with time as well as the effect of the scale  $\phi_*$  is evident. The solid blue lines are the instantaneous value of the equation of state while the red dotted line is the averaged value over a period of inflaton oscillation. Time is measured in unit of their respective scale  $m$  hence to facilitate a comparison between different models, the e-folding number is shown in the upper panel.

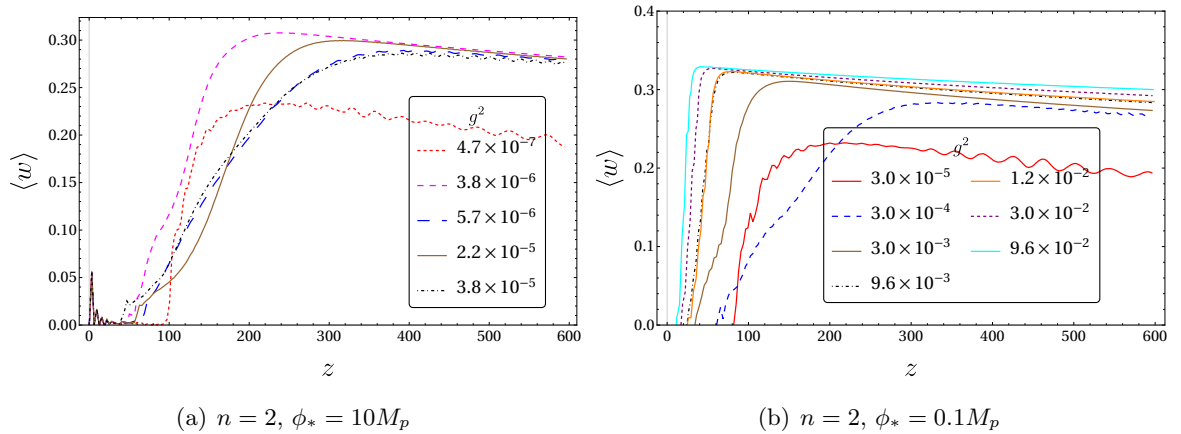


**Figure 12.** Variation of equation of state with  $g^2$  for model  $n = 2$  for the two values of  $\phi_*$ . It is evident that indefinitely increasing  $g^2$  will not bring radiation domination for  $n = 2$ .

above Rayleigh-Jeans spectrum can be easily obtained from the following bosonic distribution function defined at finite temperature  $T$  as

$$n_k = \frac{1}{\exp\left(\frac{\omega_k - \mu}{T}\right) - 1}, \quad (6.14)$$

in small chemical potential  $\mu$  limit. This implies that rather than plotting the occupation number for a particular mode, we will get a better understanding of the thermalization process by considering the combination  $\omega_k n_k$  as a function of comoving wave number  $k$  as plotted below in figs. 13 to 18 for different values  $n$ . We have, as usual, chosen the previous two values controlling scale  $\phi_*$ . The e-folding instants are chosen to cover all the three different stages of preheating discussed earlier. From the dynamics of occupation number over time, we clearly observe that with increasing  $n$ , system thermalize faster. Therefore, it would be interesting to understand this turbulent phase more closely.

For model with  $n = 2$ , during the initial linear regime of parametric resonance the IR modes are populated first. After the stationary phase, the IR modes show a greater tendency for thermalization. Nevertheless the overall spectra shows that the thermalization has not

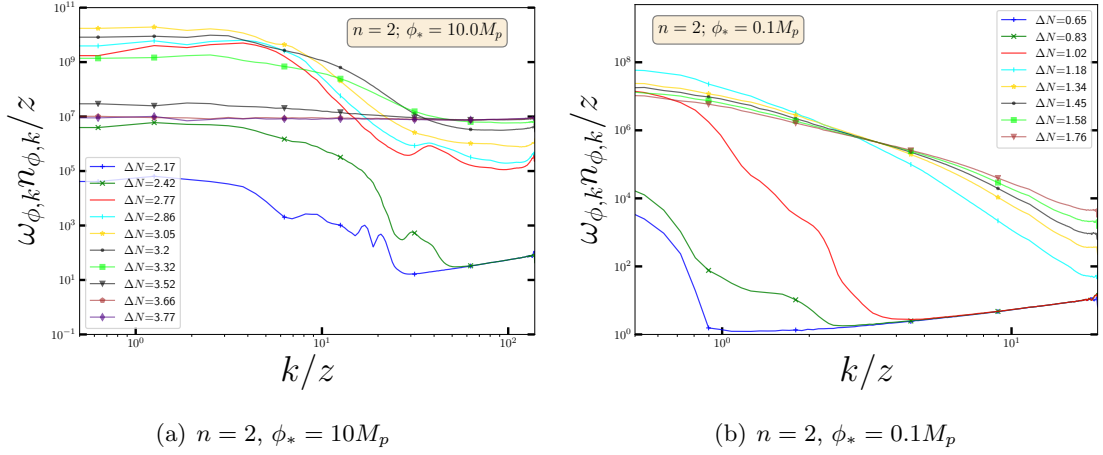


**Figure 13.** The evolution of the combination  $\omega_{\phi,k} n_{\phi,k}$  as a function of momentum  $k$  at different e-folding numbers for  $n = 2$  for the two values of  $\phi_*$

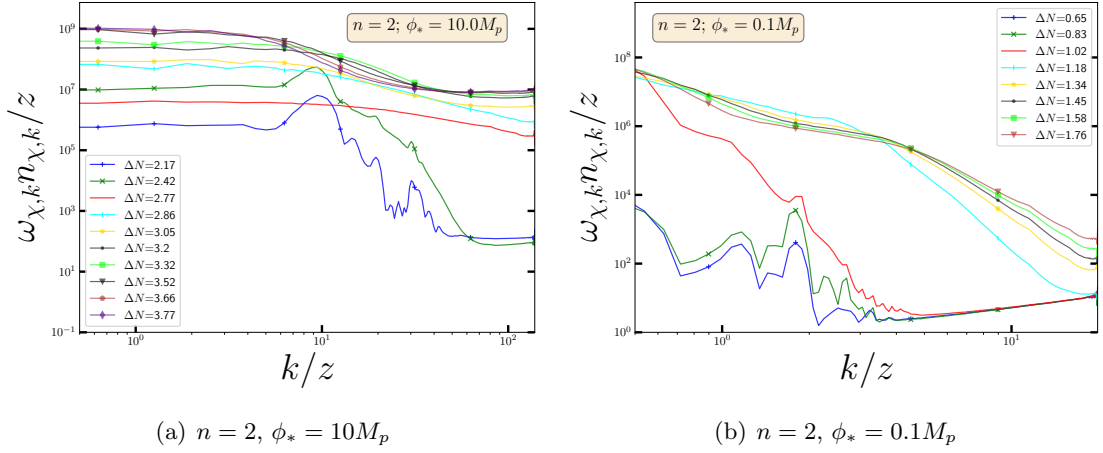


**Figure 14.** Same plot as Fig.(13) for the  $\chi$  field.

been achieved. Decreasing  $\phi_*$  do not improve the thermalization as we have seen earlier from the study of equation of state too. For  $n = 4$  the spectra after stationary phase evolve towards higher comoving momenta. But the spectra do not show thermalized behavior for  $\phi_* = 10M_p$ . Decreasing  $\phi_*$  shows a greater tendency for thermalization. For models with  $n = 6$ , the spectra is mostly flat after the initial linear stage indicating the achievement of thermalization.

Finally, we have plotted the total number densities  $n(t)$  of the two fields defined in eq. (5.12) for the models in figs. 19 to 21. Evolution of total number of particles for a particular species encodes the information about the different mechanisms responsible for changing the particle number. For example at small coupling when the particle number is small the perturbative quantum scattering process ( $\phi\chi \rightarrow \phi\chi$ ) conserves the total particle number. This particular phase can be well described by classical wave scattering known as “weak turbulence” [40]. However, as the particle number becomes large during preheating, despite small coupling, the higher order interactions may dominate, and the system move

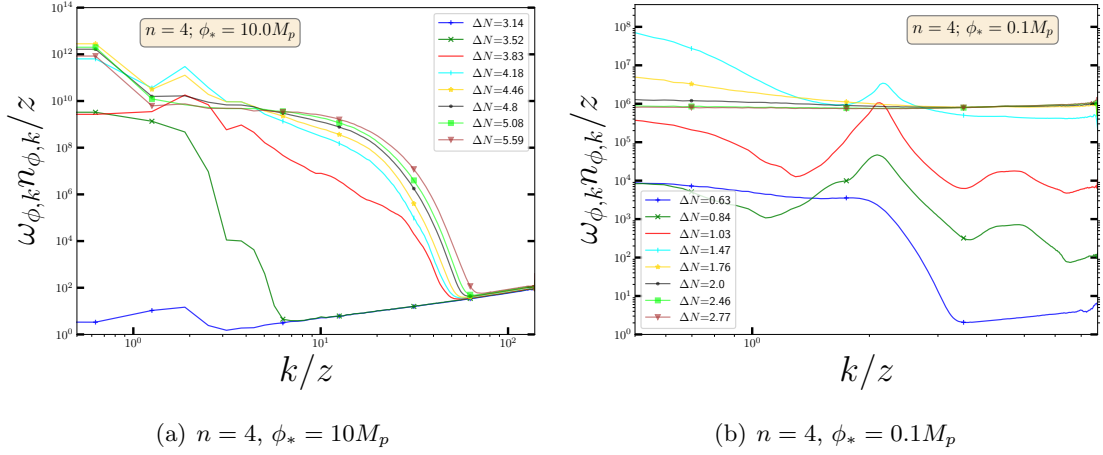


**Figure 15.** Same plot as Fig.(13) for the  $n = 4$

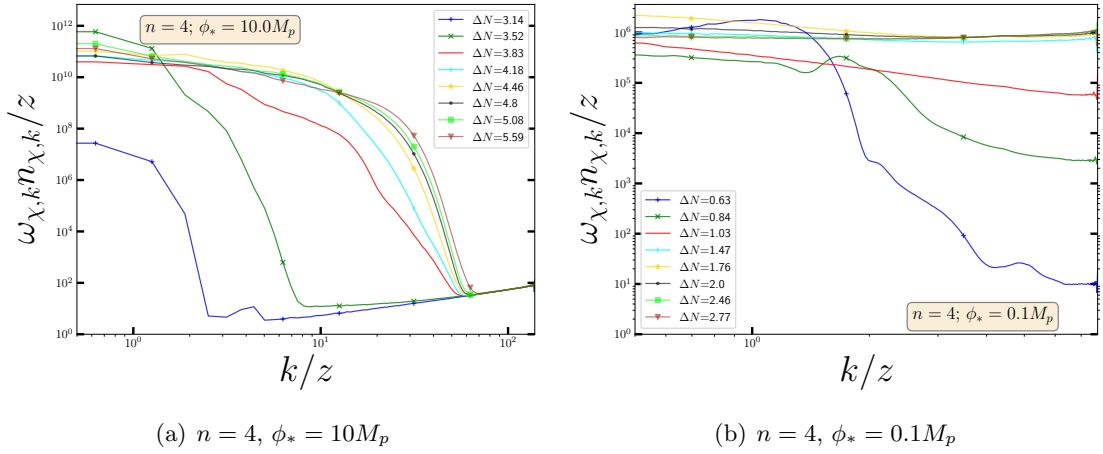


**Figure 16.** Same plot as Fig.(15) for the  $\chi$  field

towards the strong turbulence regime where total particle number will not be conserved any more. Similar to the other behaviors, the total number of particles of every individual species evolves through three distinct phases.

The particle numbers initially increases exponentially due to parametric resonance which is followed by a gradual decrease in the turbulent regime and finally settling to an asymptotic flat regime during the stationary phase. The gradual decrease is due to the fact that during the turbulent regime the occupation number shifts from low to higher momentum thereby decreasing the overall number. Although in reality, such a flow towards UV modes should also be compensated with a opposite flow. However, such a flow towards IR modes are absent in the lattice simulation due to the finite size of the box. For,  $n = 2$ , the total number for the two fields do not became identical at the end of stationary phase. For,  $n = 4$  decreasing  $\phi_*$  make the two spectra identical. For  $n = 6$  the total number for the two fields reaches the same value after the stationary phase for both the value of  $\phi_*$ . This feature is consistent with our previous conclusion that for  $n = 2$  model, the system is not fully thermalized at the end

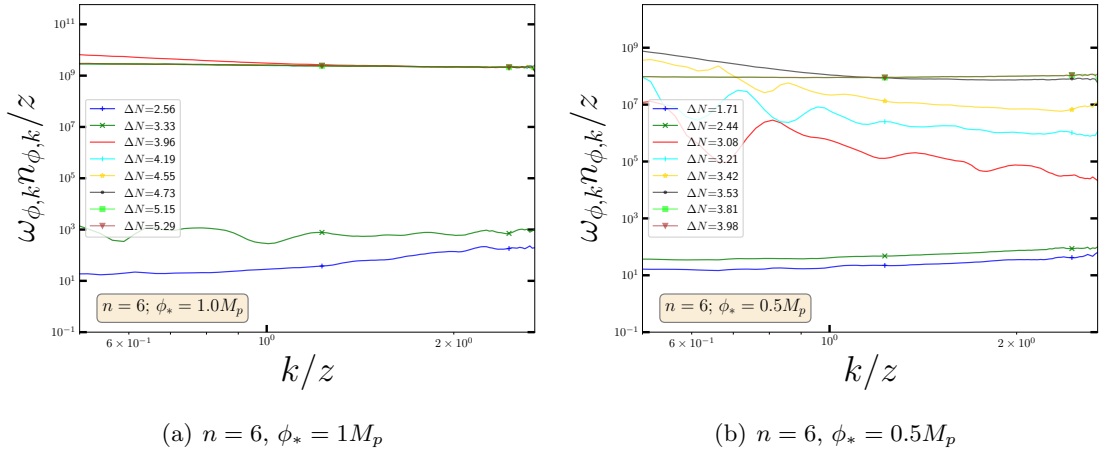


**Figure 17.** Same plot as Fig.(13) for the  $n = 6$ . In the inset we have zoomed in the higher values of the UV regime.

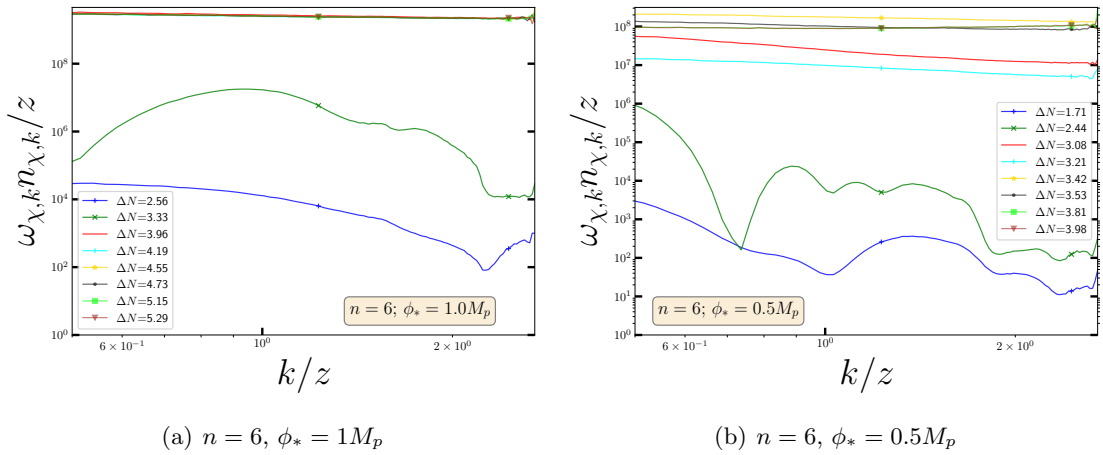
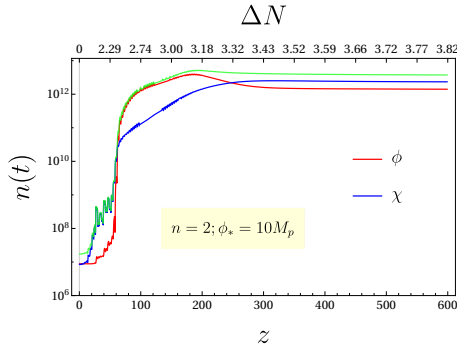


**Figure 18.** Same plot as Fig.(17) for the  $\chi$  field

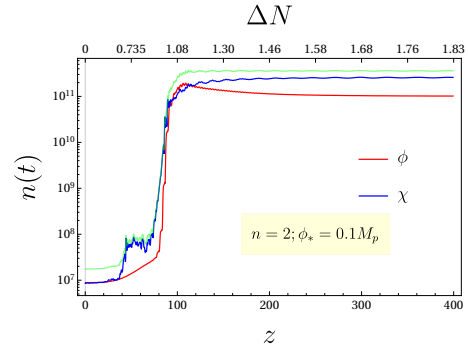
of preheating.

#### 6.4 Perturbative reheating and constraints from CMB

The purpose of the reheating phase is to create a correct initial condition for the standard big-bang. Therefore, after the end of reheating the final dominating energy component should be radiation with the characteristic equation of state  $w = 1/3$ . As we have seen for models with  $n > 2$ , the preheating is sufficient to obtain the radiation component with the required equation of state. However, it is important to remember that final state of preheating is a combination of two radiation like fluids with approximately 50% of it is inflaton field itself. Therefore, even though it behaves like a radiation, in order to connect with the CMB, one needs to consider further decay of inflaton into radiation by perturbative interaction. In any case for  $n = 2$  models we have seen that the final equation of state is not that of radiation. For long time simulation we have seen that  $w \rightarrow 0.1$  for  $n = 2$  model. As we have mentioned that we need further perturbative decay of inflation to complete the reheating and set the

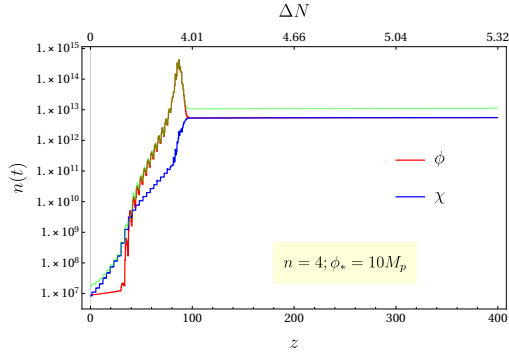


(a)  $n = 2, \phi_* = 10M_p$

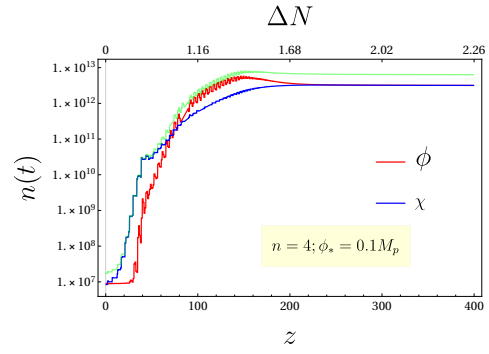


(b)  $n = 2, \phi_* = 0.1M_p$

**Figure 19.** Total number density for  $n = 2$  with  $\phi_* = (10M_p, 0.1M_p)$  Red, blue and green lines corresponds to  $n_t^\phi$ ,  $n_t^\chi$  and  $(n_t^\phi + n_t^\chi)$  respectively.

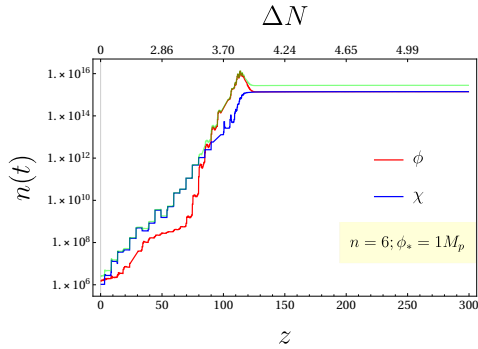


(a)  $n = 4, \phi_* = 10M_p$

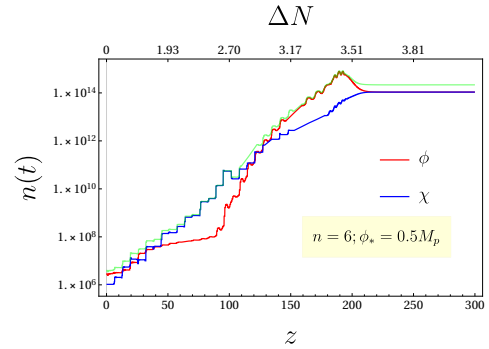


(b)  $n = 4, \phi_* = 0.1M_p$

**Figure 20.** Total number density for  $n = 4$  with  $\phi_* = (10M_p, 0.1M_p)$



(a)  $n = 6, \phi_* = 1M_p$



(b)  $n = 6, \phi_* = 0.5M_p$

**Figure 21.** Total number density for  $n = 6$  with  $\phi_* = (1M_p, 0.5M_p)$

correct initial condition for the big-bang. We have already mentioned before that to obtain the radiation domination, a three-legs interaction such  $\phi\chi^2$  will be important. The full numerical

lattice simulation considering both the interaction term will be considered in our subsequent paper. At this point we may attempt an alternative approach that will also help us to connect the reheating phase with CMB. We will follow the formalism developed in our recent papers [59] generalizing the works in [58] for decaying inflaton. In our following analysis, we will assume the decay of total energy density  $\rho_t$  whose initial value will be identified with the value obtained after the end of preheating. For  $n = 2$  we consider the equation of state to be  $w_{dec} \sim 0.22$ . If we introduce a phenomenological decay term for total energy decay we may write

$$\begin{aligned}\dot{\rho}_t + 3H(1 + w_{dec})\rho_t + \Gamma\rho_t &= 0, \\ \dot{\rho}_R + 4H\rho_R - \Gamma\rho_t &= 0,\end{aligned}\tag{6.15}$$

where  $\rho_R$  is the additional radiation energy density.

In terms of following dimensionless variables

$$\Phi = \frac{a^{3(1+w_{dec})}\rho_t}{a_I^{3(1+w_{dec})}\rho_I}; \quad R = \frac{a^4\rho_R}{a_I^3\rho_I},\tag{6.16}$$

the above equations for energy densities transformed into

$$\Phi'(N) + \frac{\Gamma}{\mathbb{H}}\Phi(N) = 0,\tag{6.17}$$

$$R'(N) - \frac{\Gamma}{\mathbb{H}}e^{(1-3w_{dec})N}\Phi(N) = 0,\tag{6.18}$$

where ‘‘prime’’ is taken with respect to e-folding ‘‘N’’ which is obtained from the Hubble equation

$$3M_p^2\mathbb{H}^2 = \rho_I \left[ \frac{\Phi(N)}{e^{3(1+w_{dec})N}} + \frac{R(N)}{e^{4N}} \right]\tag{6.19}$$

This equation could be easily solved for a given inflaton decay constant.

As mentioned, one of our main goal is to understand the direct constraints coming from CMB. A given cosmological scale  $k = a_k H_k$  which exits the horizon inflation with scale factor  $a_k$  and re-enters the horizon with the scale factor  $a_0$  at the present time, satisfies the following relation,

$$N_k + N_{\text{pre}} + N_{\text{re}}^{\text{pert}} + \ln\left(\frac{a_0}{a_{\text{re}}}\right) + \ln\left(\frac{k}{a_0 H_k}\right) = 0,\tag{6.20}$$

where  $(N_k, N_{\text{pre}}, N_{\text{re}}^{\text{pert}})$  are the inflationary, preheating and perturbative reheating e-folding number respectively.  $a_{\text{re}}$  is the scale factor after the end of perturbative reheating. Assuming that the entropy is preserved after reheating implies

$$g_{\text{re}}T_{\text{re}}^3 = \left(\frac{a_0}{a_{\text{re}}}\right)^3 \left(2T_0^3 + 6 \times \frac{7}{8}T_{\nu,0}^3\right),\tag{6.21}$$

where,  $T_0 = 2.725K$  is the present CMB temperature,  $T_{\nu,0} \sim (4/11)^{1/3}T_0$  is the present neutrino temperature and  $g_{\text{re}}$  is the effective degrees of freedom at reheating. Using the usual definition of radiation temperature,  $T_{\text{re}} = (30/g_{\text{re}}\pi^2)^{1/4}\rho_I^{1/4}(R_{\text{re}}/e^{4N_{\text{re}}})^{1/4}$  one arrives at the

following relation two equation for reheating temperature  $T_{re}$  and  $N_{re}$  in terms of other known parameters,

$$\begin{aligned} T_{re} &= \left( \frac{43}{11g_{s,re}} \right)^{1/3} \left( \frac{a_0 T_0}{k} \right) H_k e^{N_k} e^{N_{pre}} e^{N_{re}^{pert}} \\ N_{re}^{pert} &= \ln \left( \frac{a_{re}}{a_{pre}} \right). \end{aligned} \quad (6.22)$$

Where,  $a_{pre}$  is the scale factor after the end of preheating. We will solve equation 6.18 keeping the effective decay width as free parameter. The value of the effective decay width is chosen such that  $N_{re}^{pert}(\Gamma), T_{re}(\Gamma)$  satisfies Eqs.6.22.

The preheating and consequently the initial conditions for the perturbative reheating dynamics modeled by eqs.6.15 (fraction of inflaton energy density) turned out to be largely independent of the inflationary parameters  $(n_s, N_k)$  given a particular model. For  $n = 2$  model, this important fact fixes the value of  $N_{pre} \sim 1.5$  for  $\phi_* = 0.1$ , and  $N_{pre} \sim 3.5$  for  $\phi_* = 10$ . Therefore, subsequent dynamics will fix the value of  $N_{re} = N_{pre} + N_{re}^{pert}$  supplemented by the conditions eqs.6.22. Since the reheating temperature is an exponential function of e-folding number, small change in  $N_k$  or  $n_s$  significantly effects the value of  $(N_{re}, T_{re})$ . In fig.22, we have shown the dependence of  $N_{re}$  and  $T_{re}$  on the spectral index  $n_s$  for the two values of  $\phi_*$ . The dashed lines are the results from the conventional reheating constraint analysis in which complete dynamics of reheating phase is parameterized by an effective equation of state [58](for  $n = 2$ ). The solid lines is our present result. We can clearly see the significant difference in  $(T_{re}, N_{re})$  for a particular value of  $n_s$ . The total reheating phase is parametrized by the sum of e-folding numbers due to preheating  $N_{pre}$  and the perturbative reheating  $N_{re}^{pert}$ . In our case, the instantaneous reheating is thus not possible as for  $N_{re}^{pert} \rightarrow 0$ ,  $N_{re} \rightarrow N_{pre}$ . Most importantly pre-heating dynamics restricts the value of  $n_s$  within a very narrow range of  $0.971 < n_s < 0.973$  for  $\phi_* = 0.1 M_p$ . For  $\phi_* = 10 M_p$ , the range approximately is  $0.9658 < n_s < 0.9678$ . For both the cases the reheating temperature can take a wide range of values with a maximum limit to be  $T_{re}^{max} \simeq 10^{13} \sim 10^{16}$  GeV. All these constraints are based on our naive solution of Boltzmann equation.

However, let us remind the reader that inflaton decay constant  $\Gamma$  should not take arbitrary value. For a given interacting model it will have a theoretical constraints. Those are shown as shaded region in the  $(n_s, T_{re})$  plot for the given interaction discussed below. We will consider a particular Yukawa type interaction between the inflaton and a fermion

$$\mathcal{L}_{int} \supset -h\phi\bar{\psi}\psi. \quad (6.23)$$

However, the following discussions will same for other type of three point interaction with some quantitative differences. In this case the decay rate will be given by[57]

$$\Gamma = \frac{h^2 m_\phi}{8\pi} \quad (6.24)$$

where  $m_\phi$  is the tree-level mass of  $\phi$ . However, in order for our discussion to be valid we need to make sure that the effect of this coupling should be insignificant during the preheating phase. For this we note that, the effect of resonance will be appreciable when the decay rate is greater than the Hubble parameter at the beginning of preheating[24, 60]. i.e.,

$$q_f^2 m_\phi > H. \quad (6.25)$$

Where  $q_f$  is the resonance parameter in case of fermionic preheating analogous to the resonance parameter  $q$  appeared in eq. (4.3) and for the interaction term in eq. (6.23) is given by [61]

$$q_f = \frac{h^2 \phi_0^2}{m_\phi^2} \quad (6.26)$$

Combining eq. (6.25) and eq. (6.26), we obtain the condition on the coupling  $h$  when the resonance will be effective as

$$h > \left[ \frac{V(\phi_0)^{\frac{1}{2}} m_\phi^3}{3^{\frac{1}{2}} M_{\text{P}} \phi_0^4} \right]^{\frac{1}{4}} \quad (6.27)$$

This lower limit on  $h$  in turn will give us a lower limit in inflaton decay constant  $\Gamma$ . In the Fig. fig. 22 red dashed line correspond to the aforementioned limit in terms of reheating temperature. Therefore, a significant part of our result that is represented by solid blue lines is in the non-perturbative region, which we may not be trusted. However, one can make progress by fitting our results (blue lines) with an effective equation of state defined during the entire reheating phase [58], with a simple evolution equation of total energy density  $\rho = \rho_0 a^{-(1+3w_{\text{eff}})}$ , and the approximate result (dotted blue lines) turned out to be  $w_{\text{eff}} = (0.195, 0.251)$  for  $\phi_* = (10M_{\text{p}}, 0.1M_{\text{p}})$  respectively. Now the dotted line can be valid in the non-perturbative yellow region shown in the fig. 22 with an effective equation of state. To this end we must mention that the origin of the decay term in eq. (6.15) is phenomenological thus we are free to chose any interaction terms thereby the bound shown in fig. 22 can be significantly modified due to different coupling.

## 7 Conclusion and Outlook

In this work, we have studied in detail the preheating dynamics for a specific class of plateau type inflationary potential proposed by us. As we have shown earlier, these type of plateau potentials are fit will with the cosmological observation. The plateau potential in the present context can be thought of as a generalization of the chaotic power law potentials. Indeed the potential reduces to the form  $V(\phi) \propto \phi^n$  around the minimum of the potential. However, we have a scale  $\phi_*$  in our model that controls the height and width of the potential. In the present work we have explored in detail the effect of this scale on the preheating dynamics for different inflationary model parameterized by  $n = (2, 4, 6)$ . Lower the value of  $\phi_*$  the reheating dynamics attains its saturation faster. Even though qualitative behavior remains same for all the model. However, some important microscopic detail changes which are worth studying in future. In order to do comparative study we keep same value of  $g^2$  for different  $\phi_*$ . Below we list some of the important findings of our study,

- (a) Given a particular model with fixed  $(n, g^2)$ , decreasing  $\phi_*$  makes the energy transfer efficient by reducing the e-folding number.
- (b) However at the end of preheating, the total energy is distributed almost equally among the different fields taking part in the reheating dynamics. This distribution is nearly independent of the all the model parameters. Microscopic detail of the dynamics will be dependent upon the parameter. For  $n = 2$  this energy distribution is little asymmetric mainly due mass of the inflaton.

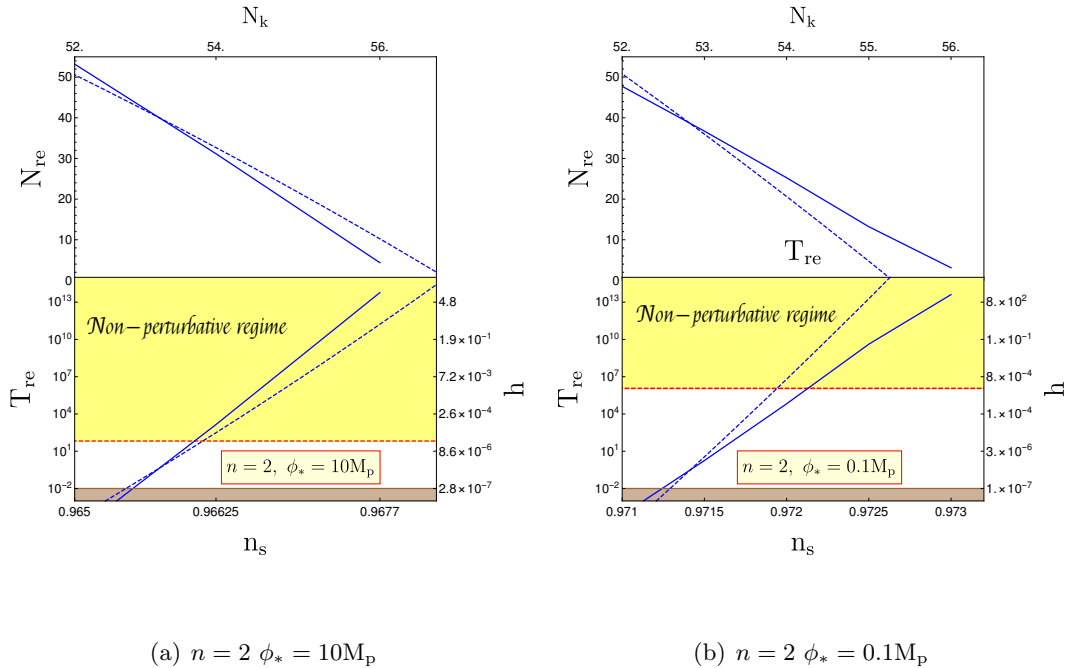


**Figure 22.** Evolution  $N_{\text{re}}$  and  $T_{\text{re}}$  with  $n_s$  for  $n = 2$  with two values of  $\phi_*$  as before. The shaded region is the region when the value of  $h$  such that the non-perturbative effects will be important. The dashed lines are the predictions from the conventional approach when the expansion during reheating phase is parameterized by an effective equation of state parameter  $w_{\text{eff}} = (0.195, 0.251)$  for  $\phi_* = (10, 0.1)M_p$ . The lower brown shaded region is below  $10\text{MeV}$  that is excluded from the constraints of big bang nucleosynthesis.

- (c) Most importantly for the models  $n = 4, 6$ , the final equation of state turns out to be that of radiation  $w = 1/3$  independent of all the other parameters. Similar observation has been made in the recent paper [54] considering the self resonance of the inflaton. For our case resonance will occur for both the fields  $(\phi, \chi)$ . We believe this is true for any model with  $n > 2$ , and for all those model final equation of state will be that of radiation. For  $n = 2$  model, however, dynamics is little difference. For this model self resonance is inefficient. The parameter  $m$  plays the role of mass of the inflaton. Therefore, at the end of preheating, inflaton behave like a non-relativistic massive particle with a little asymmetric energy distribution with the relativistic  $\chi$ -particle. Therefore, the total equation state never reaches to that of radiation in the saturation phase.
- (d) From the microscopic point of view, we found that the transition from homogeneous inflaton equation of state  $w = (n - 2)/(n + 2)$  to that of the saturated preheating equation of state  $w_{st}$  depends on  $(n, \phi_*)$ . For  $n = 2$ , with the decreasing  $\phi_*$  the transition from  $w = 0 \rightarrow w_{st} = 0.1$  becomes instantaneous. Therefore, the system must go through highly chaotic phase. On the other hand for  $n = 6$ , the opposite phenomena happens, with the increasing  $\phi_*$  the transition from  $w = 2/3 \rightarrow w_{st} = 1/3$  becomes instantaneous. This transition of equation of state happens occurs in the phase when transfer of energy from inflaton to reheating field is efficient. Therefore, all the interesting non-equilibrium phenomena such as chaos, turbulence, thermalization will happen in this phase. Thus, homogeneous inflaton equation of state plays very important role

for those non-equilibrium processes during preheating. Detailed study of this phase will be done in future.

It is apparent that the preheating itself is not the full story of the reheating dynamics. As nearly half of the total energy density is stored in the form of inflaton, we need further mechanism to get the complete transfer of inflaton energy to radiation phase, that will set the initial condition for the standard big-bang. Since we need the complete decay of inflaton, three legs interaction[41] may be important. With these kind of new interaction has been discussed in [62–64]. A three legs interaction will also necessitate incorporating the self-interaction term such as  $\lambda_\chi\chi^4$  that makes the potential bounded from below. Depending upon the value of  $\lambda_\chi$ , most of the energy density may or may not be converted into  $\chi$  quanta before the back-reaction effect will become dominant[63] in the preheating dynamics. However, during the initial stage of preheating the four-legs interaction will be dominant over the three-legs. If both the interactions are present, we will have several interesting behavior of the system[63, 64]. We will look into those effects in a separate work. In the present work, we have considered the usual perturbative decay of inflaton with a phenomenological decay term. This helped us to connect the reheating phase with CMB. Considering  $n = 2$  model, our naive analysis of Boltzmann equation limits the value of the spectral index within  $0.971 < n_s < 0.973$  for  $\phi_* = 0.1 M_p$ , and  $0.9658 < n_s < 0.9678$  for  $\phi_* = 10 M_p$ . In the above estimation, the reheating temperature is considered to be within  $10\text{MeV} < T_{re} < 10^{15}\text{GeV}$ . Finally we discussed qualitatively on the bound on the reheating temperature by looking at the non-perturbative limit on inflation decay constant  $\Gamma$  which is assumed to be originated from the Yukawa interaction between the inflaton and fermion field. As we have seen that the upper limit on the Yukawa coupling below which the perturbative analysis can be carried put a maximum bound on the reheating temperature for the models under consideration. The maximum reheating temperature has been found to be  $T_{re} \sim 10^2\text{GeV}$  with  $n_s^{\text{max}} \sim 0.966$  for  $\phi_* = 10M_p$  and  $T_{re} = 10^6\text{GeV}$  with  $n_s^{\text{max}} = 0.972$  for  $\phi_* = 0.1M_p$ . For higher values of coupling Yukawa coupling  $h$  when perturbative analysis can not be trusted, we can obtain the qualitative result considering the effective equation of state  $w_{\text{eff}}$  that can qualitatively fit our results.

However important point we should understand that there is no unified description of both the perturbative and non-perturbative reheating process. In our present analysis we have considered those as two separate phenomena connected by the initial condition for the Boltzmann equation after the end of preheating. Therefore, it would be interesting to understand those in a single framework. Another important issue we have not discussed is related to incomplete decay of inflaton for  $n > 2$  models where final equation of state becomes  $1/3$  after preheating. For these cases simple Boltzmann description of perturbative reheating becomes untenable for  $(T_{re}, N_{re})$ . Therefore for such situation how and when the actual radiation domination starts, will be an important question to discuss.

## 8 Acknowledgement

We also thank our HEP and Gravity group members for their valuable comments and discussions. PS would like to thank Gary Felder for help during various steps with LATTICEASY

## References

- [1] A. A. Starobinsky, “A New Type of Isotropic Cosmological Models Without Singularity,” *Phys. Lett.*, vol. B91, pp. 99–102, 1980. [,771(1980)].
- [2] D. Kazanas, “Dynamics of the Universe and Spontaneous Symmetry Breaking,” *Astrophys. J.*, vol. 241, pp. L59–L63, 1980.
- [3] K. Sato, “First Order Phase Transition of a Vacuum and Expansion of the Universe,” *Mon. Not. Roy. Astron. Soc.*, vol. 195, pp. 467–479, 1981.
- [4] A. H. Guth, *Phys. Rev. D* **23**, 347356 (1981).
- [5] A. D. Linde, *Phys. Lett. B* **108**, 389393 (1982).
- [6] A. Albrecht and P. J. Steinhardt, *Phys. Rev. Lett.* **48**, 12201223 (1982).
- [7] C. Cheung, P. Creminelli, A. L. Fitzpatrick, J. Kaplan and L. Senatore, *JHEP* **0803**, 014 (2008) [arXiv:0709.0293 [hep-th]].
- [8] S. Weinberg, *Phys. Rev. D* **77**, 123541 (2008) [arXiv:0804.4291 [hep-th]].
- [9] D. Boyanovsky, *Phys. Rev. D* **92**, no. 2, 023527 (2015) [arXiv:1506.07395 [astro-ph.CO]].
- [10] D. Boyanovsky, *Phys. Rev. D* **93**, 043501 (2016) [arXiv:1511.06649 [astro-ph.CO]].
- [11] V. Mukhanov, *Physical foundations of cosmology*, Cambridge University Press, 2005.
- [12] J. Martin, C. Ringeval and V. Vennin, *Phys. Dark Univ.* **5-6**, 75 (2014) [arXiv:1303.3787 [astro-ph.CO]].
- [13] Planck Collaboration: P. A. R. Ade et al., Planck 2013 results. XXII. Constraints on Inflation, *Astron. Astrophys.* **571** (2014) A22, [arXiv:1303.5082 [astro-ph.CO]]; Planck Collaboration: P. A. R. Ade et al., Planck 2015 results. XX. Constraints on Inflation, *Astron. Astrophys.* **594**, A20 (2016), [arXiv:1502.02114 [astro-ph.CO]]; P. A. R. Ade et al. [BICEP2/Keck, Planck Collaborations]. *Rev. Lett.* **114**, 101301 (2015) [arXiv:1502.00612 [astro-ph.CO]].
- [14] Keck Array, BICEP2 Collaborations: P. A. R. Ade et al., BICEP2 / Keck Array VI: Improved Constraints On Cosmology and Foregrounds When Adding 95 GHz Data From Keck Array, *Phys. Rev. Lett.* **116**, 031302 (2016), [arXiv:1510.09217 [astro-ph.CO]].
- [15] D. Maity and P. Saha, arXiv:1610.00173 [astro-ph.CO].
- [16] Y. Akrami *et al.* [Planck Collaboration], arXiv:1807.06211 [astro-ph.CO].
- [17] D. Maity and P. Saha, arXiv:1804.10115 [hep-ph].
- [18] A. Albrecht, P. J. Steinhardt, M. S. Turner and F. Wilczek, *Phys. Rev. Lett.* **48** (1982) 1437.
- [19] A. D. Dolgov and A. D. Linde, *Phys. Lett.* **116B** (1982) 329.
- [20] L. F. Abbott, E. Farhi and M. B. Wise, *Phys. Lett.* **117B** (1982) 29.
- [21] J. H. Traschen and R. H. Brandenberger, *Phys. Rev. D* **42** (1990) 2491.
- [22] L. Kofman, A. D. Linde and A. A. Starobinsky, *Phys. Rev. Lett.* **73** (1994) 3195 [hep-th/9405187].
- [23] Y. Shtanov, J. H. Traschen and R. H. Brandenberger, *Phys. Rev. D* **51** (1995) 5438 [hep-ph/9407247].
- [24] L. Kofman, A. D. Linde and A. A. Starobinsky, *Phys. Rev. D* **56** (1997) 3258 [hep-ph/9704452].
- [25] P. B. Greene, L. Kofman, A. D. Linde and A. A. Starobinsky, *Phys. Rev. D* **56**, 6175 (1997) [hep-ph/9705347].
- [26] L. D. Landau and E. M. Lifshitz, *Mechanics* (Butterworth-Heinemann; 1982 )

- [27] B. A. Bassett, S. Tsujikawa and D. Wands, *Rev. Mod. Phys.* **78** (2006) 537 [astro-ph/0507632].
- [28] R. Allahverdi, R. Brandenberger, F. Y. Cyr-Racine and A. Mazumdar, *Ann. Rev. Nucl. Part. Sci.* **60** (2010) 27 [arXiv:1001.2600 [hep-th]].
- [29] M. A. Amin, M. P. Hertzberg, D. I. Kaiser and J. Karouby, *Int. J. Mod. Phys. D* **24** (2014) 1530003 [arXiv:1410.3808 [hep-ph]].
- [30] G. F. Giudice, M. Peloso, A. Riotto and I. Tkachev, *JHEP* **9908** (1999) 014 doi:10.1088/1126-6708/1999/08/014 [hep-ph/9905242].
- [31] G. F. Giudice, A. Riotto and I. Tkachev, *JHEP* **9911** (1999) 036 doi:10.1088/1126-6708/1999/11/036 [hep-ph/9911302].
- [32] R. Allahverdi and M. Drees, *Phys. Rev. Lett.* **89** (2002) 091302 doi:10.1103/PhysRevLett.89.091302 [hep-ph/0203118].
- [33] R. Allahverdi and M. Drees, *Phys. Rev. D* **66** (2002) 063513 doi:10.1103/PhysRevD.66.063513 [hep-ph/0205246].
- [34] E. W. Kolb, A. Notari and A. Riotto, *Phys. Rev. D* **68** (2003) 123505 doi:10.1103/PhysRevD.68.123505 [hep-ph/0307241].
- [35] R. Kallosh and A. Linde, *JCAP* **1307**, 002 (2013) [arXiv:1306.5220 [hep-th]]; S. Ferrara, et al, *Phys. Rev. D* **88**, 8, 085038 (2013) [arXiv:1307.7696 [hep-th]]; R. Kallosh, A. Linde and D. Roest, *JHEP* **1311**, 198 (2013) [arXiv:1311.0472 [hep-th]]; S. Cecotti and R. Kallosh, *JHEP* **1405**, 114 (2014) [arXiv:1403.2932 [hep-th]].
- [36] N. W. McLachlan, *Theory and Application of Mathieu Functions*, Dover Publications (1964)
- [37] W. Magnus and S. Winkler. *Hill's equation*, Dover Publications (1979) Series
- [38] G. N. Felder and I. Tkachev, *Comput. Phys. Commun.* **178** (2008) 929 doi:10.1016/j.cpc.2008.02.009 [hep-ph/0011159].
- [39] G. N. Felder, *Comput. Phys. Commun.* **179** (2008) 604 [arXiv:0712.0813 [hep-ph]].
- [40] G. N. Felder and L. Kofman, *Phys. Rev. D* **63**, 103503 (2001) [hep-ph/0011160].
- [41] D. I. Podolsky, G. N. Felder, L. Kofman and M. Peloso, *Phys. Rev. D* **73**, 023501 (2006) [hep-ph/0507096].
- [42] K. D. Lozanov and M. A. Amin, *Phys. Rev. D* **97** (2018) no.2, 023533 [arXiv:1710.06851 [astro-ph.CO]].
- [43] D. G. Figueroa and F. Torrenti, *JCAP* **1702**, no. 02, 001 (2017) [arXiv:1609.05197 [astro-ph.CO]].
- [44] S. Y. Khlebnikov and I. I. Tkachev, *Phys. Rev. Lett.* **77**, 219 (1996) [hep-ph/9603378].
- [45] T. Prokopec and T. G. Roos, *Phys. Rev. D* **55**, 3768 (1997) [hep-ph/9610400].
- [46] A. V. Frolov, *JCAP* **0811**, 009 (2008) [arXiv:0809.4904 [hep-ph]].
- [47] R. Easther, H. Finkel and N. Roth, *JCAP* **1010**, 025 (2010) [arXiv:1005.1921 [astro-ph.CO]].
- [48] Z. Huang, *Phys. Rev. D* **83**, 123509 (2011) [arXiv:1102.0227 [astro-ph.CO]].
- [49] M. S. Turner, *Phys. Rev. D* **28**, 1243 (1983).
- [50] R. Micha and I. I. Tkachev, *Phys. Rev. Lett.* **90**, 121301 (2003) [hep-ph/0210202].
- [51] R. Micha and I. I. Tkachev, *Phys. Rev. D* **70**, 043538 (2004) [hep-ph/0403101].
- [52] M. P. Hertzberg, J. Karouby, W. G. Spitzer, J. C. Becerra and L. Li, *Phys. Rev. D* **90**, 123528 (2014) [arXiv:1408.1396 [hep-th]].

- [53] M. P. Hertzberg, J. Karouby, W. G. Spitzer, J. C. Becerra and L. Li, Phys. Rev. D **90**, 123529 (2014) [arXiv:1408.1398 [hep-th]].
- [54] K. D. Lozanov and M. A. Amin, Phys. Rev. Lett. **119**, no. 6, 061301 (2017) [arXiv:1608.01213 [astro-ph.CO]].
- [55] G. N. Felder and L. Kofman, Phys. Rev. D **75**, 043518 (2007) [hep-ph/0606256].
- [56] G. N. Felder and O. Navros, JCAP **0702**, 014 (2007) [hep-ph/0701128].
- [57] M. E. Peskin and D. V. Schroeder, “An Introduction to Quantum Field Theory,” Addison Wesley (Reading, Mass), 1995
- [58] J. Martin and C. Ringeval, Phys. Rev. **D82**, 023511 (2010); J. Martin, C. Ringeval and V. Vennin, Phys. Rev.Lett. **114**, 081302 (2015); L. Dai, M. Kamionkowski and J. Wang, Phys. Rev. Lett. **113**, 041302 (2014).
- [59] D. Maity, ArXiv:1709.00251; D. Maity, P Saha, arXiv:1801.03059,
- [60] M. Drewes, J. U. Kang and U. R. Mun, JHEP **1711**, 072 (2017) [arXiv:1708.01197 [astro-ph.CO]].
- [61] P. B. Greene and L. Kofman, Phys. Lett. B **448**, 6 (1999) doi:10.1016/S0370-2693(99)00020-9 [hep-ph/9807339].
- [62] N. Shuhmaher and R. Brandenberger, Phys. Rev. D **73**, 043519 (2006) [hep-th/0507103].
- [63] J. F. Dufaux, G. N. Felder, L. Kofman, M. Peloso and D. Podolsky, JCAP **0607**, 006 (2006) [hep-ph/0602144].
- [64] A. A. Abolhasani, H. Firouzjahi and M. M. Sheikh-Jabbari, Phys. Rev. D **81**, 043524 (2010) [arXiv:0912.1021 [hep-th]].